



Match-up database Analyses Report

SMOS SSS L2 v700 (ESA)

TSG (SAMOS)

SPURS 2

prepared by the Pi-MEP Consortium

December 15, 2024

Contents

1	Overview	6
2	The MDB file datasets	7
2.1	Satellite SSS product	7
2.1.1	SMOS SSS L2 v700 (ESA)	7
2.2	<i>In situ</i> SSS dataset	10
2.3	Auxiliary geophysical datasets	11
2.3.1	CMORPH	11
2.3.2	ASCAT	12
2.3.3	ISAS	12
2.3.4	World Ocean Atlas Climatology	13
2.4	Overview of the Match-ups generation method	13
2.4.1	<i>In situ</i> /Satellite data filtering	13
2.4.2	<i>In situ</i> /Satellite Co-localization	13
2.4.3	MDB pair Co-localization with auxiliary data and complementary information	14
2.4.4	Content of the Match-Up NetCDF files	15
2.5	MDB characteristics for each specific <i>in situ</i> /satellite pair	15
2.5.1	Number of paired SSS data as a function of time and distance to coast	15
2.5.2	Histograms of the SSS match-ups	16
2.5.3	Distribution of <i>in situ</i> SSS depth measurements	16
2.5.4	Spatial Distribution of Match-ups	17
2.5.5	Histograms of the spatial and temporal lags of the match-ups pairs	17
3	MDB file Analyses	18
3.1	Spatial Maps of the Temporal mean and Std of <i>in situ</i> and satellite SSS and of their difference (Δ SSS)	18
3.2	Time series of the monthly median and Std of <i>in situ</i> and satellite SSS and of their difference (Δ SSS)	20
3.3	Zonal mean and Std of <i>in situ</i> and satellite SSS and of the difference (Δ SSS)	20
3.4	Scatterplots of satellite vs <i>in situ</i> SSS by latitudinal bands	21
3.5	Time series of the monthly median and Std of Δ SSS sorted by latitudinal bands	22
3.6	Δ SSS sorted as function of geophysical parameters	23
3.7	Δ SSS maps and statistics for different geophysical conditions	25
4	Summary	27
5	More Comparison/Validation Materials	29
5.1	Comparisons with other satellite products	29
5.2	Statistics derived for the different <i>in situ</i> databases	31

List of Figures

2	Number of match-ups between TSG (SAMOS) and SMOS SSS L2 v700 (ESA) SSS as a function of time (a) and as function of the distance to coast (b) over the SPURS 2 Pi-MEP region and for the full satellite product period.	15
---	---	----

3	Histograms of SSS from TSG (SAMOS) (a) and SMOS SSS L2 v700 (ESA) (b) considering all match-up pairs per bins of 0.1 over the SPURS 2 Pi-MEP region and for the full satellite product period.	16
4	Histograms of the depth of the upper level SSS measurements from TSG (SAMOS) in the Match-up DataBase for the SPURS 2 Pi-MEP region (a) and temporal mean spatial distribution of pressure of the <i>in situ</i> SSS data over $1^\circ \times 1^\circ$ boxes and for the full satellite product period (b).	16
5	Number of SSS match-ups between TSG (SAMOS) SSS and the SMOS SSS L2 v700 (ESA) SSS product for the SPURS 2 Pi-MEP region over $1^\circ \times 1^\circ$ boxes and for the full satellite product period.	17
6	Histograms of the spatial (a) and temporal (b) lags between the location/time of the TSG (SAMOS) measurement and the date of the corresponding SMOS SSS L2 v700 (ESA) SSS pixel.	18
7	Temporal mean (left) and Std (right) of SSS from SMOS SSS L2 v700 (ESA) (top), TSG (SAMOS) (middle), and of Δ SSS (Satellite - TSG (SAMOS)). Only match-up pairs are used to generate these maps.	19
8	Time series of the monthly median SSS (top), median of Δ SSS (Satellite - TSG (SAMOS)) and Std of Δ SSS (Satellite - TSG (SAMOS)) over the SPURS 2 Pi-MEP region considering all match-ups collected by the Pi-MEP.	20
9	Left panel: Zonal mean SSS from SMOS SSS L2 v700 (ESA) satellite product (black) and from TSG (SAMOS) (blue). Right panel: Zonal mean of Δ SSS (Satellite - TSG (SAMOS)) for all the collected Pi-MEP match-up pairs estimated over the full satellite product period.	21
10	Contour maps of the concentration of SMOS SSS L2 v700 (ESA) SSS (y-axis) versus TSG (SAMOS) SSS (x-axis) at match-up pairs for different latitude bands. For each plot, the red line shows $x=y$. The black thin and dashed lines indicate a linear fit through the data cloud and the $\pm 95\%$ confidence levels, respectively. The number match-up pairs n , the slope and R^2 coefficient of the linear fit, the root mean square (RMS) and the mean bias between satellite and <i>in situ</i> data are indicated for each latitude band in each plots.	22
11	Monthly median (red curves) of Δ SSS (Satellite - TSG (SAMOS)) and ± 1 Std (black vertical thick bars) as function of time for all the collected Pi-MEP match-up pairs estimated over the SPURS 2 Pi-MEP region and for the full satellite product period are shown for different latitude bands: (a) $80^\circ\text{S}-80^\circ\text{N}$, (b) $20^\circ\text{S}-20^\circ\text{N}$, (c) $40^\circ\text{S}-20^\circ\text{S}$ and $20^\circ\text{N}-40^\circ\text{N}$ and (d) $60^\circ\text{S}-40^\circ\text{S}$ and $40^\circ\text{N}-60^\circ\text{N}$	23
12	Δ SSS (Satellite - TSG (SAMOS)) sorted as function of TSG (SAMOS) SSS values (a), ISAS SSS (b), ASCAT Wind speed (c), CCMP Wind speed (d), CMORPH rain rate (e) and IMERG rain rate (f). In all plots the median and Std of Δ SSS for each bin is indicated by the red curves and black vertical thick bars (± 1 Std).	24
13	Δ SSS (Satellite - TSG (SAMOS)) sorted as function of TSG (SAMOS) SST values (a), CMC SST (b), ERA5 SST (c), AVHRR SST (d), distance to coast (e) and distance to ice edge (f). In all plots the median and Std of Δ SSS for each bin is indicated by the red curves and black vertical thick bars (± 1 Std). Links to similar figures sorted as function of Sea ice fraction and in situ measurement depth	25
14	Temporal mean gridded over spatial boxes of size $1^\circ \times 1^\circ$ of Δ SSS (SMOS SSS L2 v700 (ESA) - TSG (SAMOS)) for 5 different subdatasets corresponding to: RR=0 mm/h, $3 < U_{10} < 12$ m/s, $\text{SST} > 5^\circ\text{C}$, distance to coast > 800 km (a), RR=0 mm/h, $3 < U_{10} < 12$ m/s (b), $\text{RR} > 1\text{mm/h}$ and $U_{10} < 4\text{m/s}$ (c), WOA2013 SSS Std < 0.2 (d), WOA2013 SSS Std > 0.2 (e).	26

15	Normalized histogram of Δ SSS (SMOS SSS L2 v700 (ESA) - TSG (SAMOS)) for 5 different subdatasets corresponding to: RR=0 mm/h, $3 < U_{10} < 12$ m/s, SST>5°C, distance to coast > 800 km (a), RR=0 mm/h, $3 < U_{10} < 12$ m/s (b), RR>1mm/h and $U_{10} < 4$ m/s (c), WOA2013 SSS Std<0.2 (d), WOA2013 SSS Std>0.2 (e)	27
----	--	----

Acronym

Aquarius	NASA/CONAE Salinity mission
ASCAT	Advanced Scatterometer
ATBD	Algorithm Theoretical Baseline Document
BLT	Barrier Layer Thickness
CMORPH	CPC MORPHing technique (precipitation analyses)
CPC	Climate Prediction Center
CTD	Instrument used to measure the conductivity, temperature, and pressure of seawater
DM	Delayed Mode
EO	Earth Observation
ESA	European Space Agency
FTP	File Transfer Protocol
GOSUD	Global Ocean Surface Underway Data
GTMBA	The Global Tropical Moored Buoy Array
Ifremer	Institut français de recherche pour l'exploitation de la mer
IPEV	Institut polaire français Paul-Émile Victor
IQR	Interquartile range
ISAS	<i>In Situ</i> Analysis System
Kurt	Kurtosis (fourth central moment divided by fourth power of the standard deviation)
L2	Level 2
LEGOS	Laboratoire d'Etudes en Géophysique et Océanographie Spatiales
LOCEAN	Laboratoire d'Océanographie et du Climat : Expérimentations et Approches Numériques
LOPS	Laboratoire d'Océanographie Physique et Spatiale
MDB	Match-up Data Base
MEOP	Marine Mammals Exploring the Oceans Pole to Pole
MLD	Mixed Layer Depth
NCEI	National Centers for Environmental Information
NRT	Near Real Time
NTAS	Northwest Tropical Atlantic Station
OI	Optimal interpolation
Pi-MEP	Pilot-Mission Exploitation Platform
PIRATA	Prediction and Researched Moored Array in the Atlantic
QC	Quality control
R_{sat}	Spatial resolution of the satellite SSS product
RAMA	Research Moored Array for African-Asian-Australian Monsoon Analysis and Prediction
r^2	Square of the Pearson correlation coefficient
RMS	Root mean square
RR	Rain rate
SAMOS	Shipboard Automated Meteorological and Oceanographic System
Skew	Skewness (third central moment divided by the cube of the standard deviation)
SMAP	Soil Moisture Active Passive (NASA mission)
SMOS	Soil Moisture and Ocean Salinity (ESA mission)
SPURS	Salinity Processes in the Upper Ocean Regional Study
SSS	Sea Surface Salinity
$SSS_{in situ}$	<i>In situ</i> SSS data considered for the match-up

SSS_{SAT}	Satellite SSS product considered for the match-up
ΔSSS	Difference between satellite and <i>in situ</i> SSS at colocalized point ($\Delta SSS = SSS_{SAT} - SSS_{insitu}$)
SST	Sea Surface Temperature
Std	Standard deviation
Std*	Robust Standard deviation = $\text{median}(\text{abs}(x - \text{median}(x))) / 0.67$ (less affected by outliers than Std)
Stratus	Surface buoy located in the eastern tropical Pacific
Survostral	SURVeillance de l'Océan AuSTRAL (Monitoring the Southern Ocean)
TAO	Tropical Atmosphere Ocean
TSG	ThermoSalinoGraph
WHOI	Woods Hole Oceanographic Institution
WHOTS	WHOI Hawaii Ocean Time-series Station
WOA	World Ocean Atlas

1 Overview

In this report, we present systematic analyses of the Match-up DataBase (MDB) files generated by the Pi-MEP platform within the following Pi-MEP region and for the below pair of Satellite/*in situ* SSS data:

- Pi-MEP region: SPURS 2 (download the corresponding mask in NetCDF [here](#))
- SSS satellite product (SSS_{SAT}): SMOS SSS L2 v700 (ESA)
- *In situ* dataset ($SSS_{In situ}$): TSG (SAMOS) (download the corresponding *in situ* report [here](#))

In the following, $\Delta SSS = SSS_{SAT} - SSS_{In situ}$ denotes the difference between the satellite and *in situ* SSS at the colocalized points that form the MDB.

This report presents successively:

The MDB file DataSets (Section 2)

- A short description of the satellite SSS product considered in the match-up (2.1)
- A short description of the *in situ* SSS dataset considered in the match-up (2.2)
- A short description of the auxiliary geophysical datasets co-localized with SSS pairs (2.3)
- An overview of how the Match-ups were evaluated (2.4)
- An overview of the MDB characteristics for the particular *in situ*/satellite pairs (2.5)

The major results of the MDB file Analyses (Section 3)

- Spatial Maps of the Time-mean and temporal Std of *in situ* and satellite SSS and of the ΔSSS (3.1)
- Time series of the monthly median and Std of *in situ* and satellite SSS and of the ΔSSS (3.2)
- Zonal mean and Std of *in situ* and satellite SSS and of the ΔSSS (3.3)
- Scatterplots of satellite vs *in situ* SSS by latitudinal bands (3.4)
- Time series of the monthly median and Std of the ΔSSS sorted by latitudinal bands (3.5)
- ΔSSS sorted as function of geophysical parameters (3.6)
- ΔSSS maps and statistics for different geophysical conditions (3.7)

All analyses are conducted over the Pi-MEP Region specified above and over the full satellite SSS product period. Original figures appearing in this report can be downloaded as PNG files [here](#) or by clicking directly on the figure.

2 The MDB file datasets

2.1 Satellite SSS product

2.1.1 SMOS SSS L2 v700 (ESA)

Quality and major features of the SMOS Level 2 Sea Surface Salinity data products generated by version 700 of the Level 2OS Operational Processor (L2OS) can be found in the [SMOS-Level-2-Ocean-Salinity-v700-release-note](#). Version 700 of the Level 2 Sea Surface Salinity data product is available for the SMOS mission lifetime with the following file class and version:

File class	File version	From	To
REPR	v700	1 June 2010	24 Mai 2021
OPER	v700	25 Mai 2021	present

Measurements from the commissioning phase (12 January 2010 - 31 May 2010) show drifts due to instrument tests taking place during this period. Even though data are available (upon request) it is not advisable to use them. The SMOS data users are invited to use this new data set, which supersedes the previous one generated by the algorithm baseline version 662 and to read this note carefully to ensure optimal exploitation of the version 700 data set. Further information on the quality of the dataset can be found in the reprocessing verification report and in the validations report (available from June 2021 onwards) [here](#).

Main improvements in the L2OS version 700 data set

The major improvements introduced in the currently operational version 700 of the SMOS Level 2 sea surface salinity processor are:

1. The SSS anomaly field has been substantially revisited. The fields present in the version v662 of the products were obtained by simply subtracting the climatological SSS value contained in WOA2009 from the retrieved SMOS SSS values. Since v700, the SSS anomaly is computed against a SMOS-derived SSS climatology using 7 years of SSS retrievals (2013-2019). In order to improve quality, the SMOS-derived climatology corrects also for part of the systematic biases found in the SMOS SSS retrievals (such as land contamination). A full description of the method to produce the SMOS-based climatology appears in the section 2.2.9 of the TGRD document (see references in this release note).
2. The Somaraju and Trumpf (ST) seawater dielectric constant model has been now introduced to replace Klein and Swift's dielectric constant model that was used in the previous versions of the algorithm to estimate the specular sea surface emissivity and thus retrieve salinity. The ST model has been tuned to minimize SMOS limitations found in the SSS retrievals with the original model of ST and to improve SSS retrieval quality in cold waters with respect the Klein and Swift's dielectric constant model. This was achieved with the support of the cardioid parameters provided along with the UDP products (so called, Acard field). Further information can be found in the section 4.1.4 of the ATBD as well as in [Boutin et al. \(2020\)](#) (see references of this release note)
3. The procedure to compute the Ocean Target Transform (OTT) for systematic instrumental bias correction has now improved. In particular, a more stringent filtering is applied to reduce the level of noise in the OTT, especially in the upper part of the AF-FOV. The novel filtering stabilizes the OTT which becomes less impacted by Radio Frequency Interferences

(RFI) or errors due to TEC variations. Further details are provided in section 5.8.3 of the ATBD (see references of this release note).

4. The estimation of the theoretical retrieval error has also been improved and now is more representative of the true error. This change impacts the values of the UDP fields `Sigma_SSS_corr`, `Sigma_SSS_uncorr`, and `Sigma_SSS_anom`. For further details, reader is invited to check section 4.11.2 of the ATBD (see references of this release note).
5. An improved correction for the Land/Sea Contamination (LSC) has also now been introduced to reduce SSS retrievals biases in areas located at distances less than 1,000 km from the nearest coasts. The main differences with respect v662 is that the new method makes use of an improved reference SSS to derive the correction. Specifically, the In Situ Analysis System (ISAS-15; Gaillard et al. (2016)) derived fields are used instead of the World Ocean Atlas (WOA) Climatology fields used in previous version. A stricter RFI filtering and a gap-filling method based on an empirical convolution kernel are also applied in this latest LSC correction. These changes are meant to reduce the impact of the limitations from previous version, where areas with high natural dynamics or impacted frequently by RFI were not well represented in the correction (particularly in the tropical Atlantic). Further information is found in the section 2.2.8 of the TGRD (see references of this release note).
6. The flags defined to estimate the impact of sea-state conditions on SSS retrieval quality have been now revisited. Six flags called `Fg_sc_sea_state_n`, with $n=1, \dots, 6$, are present in the UDP files, which can be combined to filter SSS retrievals according to sea-state. These flags are based on threshold values of inverse wave eight (Ω) and swell fraction which have been now better defined and corrected to represent more accurately the presence of young seas, old seas, and swell, correspondingly. The worst SSS quality is observed for `Fg_sc_sea_state_1` (wind sea dominated old seas) and `Fg_sc_sea_state_5` (wind sea dominated young sea state). Data acquired in these conditions are less reliable. .
7. SMOS SSS retrievals from version 662 were obtained including a novel sun glint correction. The sun glint is estimated as a combination of the sun L-band radiation reflection in the ocean's surface and the impact of the surface roughness in the scattering of the signal. The modelled brightness temperature associated to sun glint within the SMOS scenes is calculated and included as part of the geophysical model function for the retrieval. In the version 700, the source of solar L-band radio fluxes has been modified, replacing the previously used rescaled Penticton datasets with an inter-calibrated L-band solar flux from on-ground radio-telescope rescaled for optimal SMOS data processing. This has proved to be a more accurate source of L-band solar fluxes for the purposes of the mission. For further details, readers are directed to section 2.4.6 and Annex A.3 from TGRD (see references of this release note).
8. Updated configuration of switches and filters used in the data processing. For further information see the section 2.4.7 of the TGRD (see references of this release note). .

The L2OS version 700 data set has been generated using a newly recalibrated L1c dataset of SMOS MIRAS Brightness Temperatures (version 724). For further details on the L1c data sets see the L1c data version 724 read-me-first note available [here](#).

L2OS version 700 performance and caveats

The reprocessed data set has been analysed by ESLs and ARGANS. The reference document is mentioned above. The main conclusions are:

- Land-sea contamination corrected salinities (SSS_corr) almost cancel the global mean bias in near-to-coast regions (> 40 km and < 800 km) as compared to SSS_uncorr. Caveats found in previous version in the tropical Atlantic Ocean and in the high northern latitudes have disappeared.
- On SSS_uncorr, land-sea contamination is still present, but with different across track signatures and it is less variable across swath.
- High latitudes of the southern hemisphere: the new dielectric constant model corrects for most positive SSS biases in descending orbits during March-August period. However, due to remaining contamination of other origin (likely sea ice contamination), positive biases still remain for the rest of the year. On ascending orbits, negative biases ~ -0.5 pss are observed all the year round.
- The new salinity anomaly product exhibit reduced systematic errors (such as land-sea contamination) compared with the previous anomaly fields which used WOA climatology as a reference. Nevertheless, systematic seasonal latitudinal errors are not corrected in this version and generate artefacts.
- Ascending-descending differences in retrieved SSS remain, but they are more homogeneous spatially than in the previous version. We noticed stronger sea-ice contamination in the southern ocean on ascending orbits than in previous version.

Filtering retrievals

We strongly recommend users to filter L2OS sea surface salinity retrievals using the procedure detailed below. The list of flags recommended to use for data filtering is as follows:

Table 1: List of recommended flags

Flag	Rejection condition
Fg_ctrl_ecmwf	0
Fg_ctrl_num_meas_min	1
Fg_ctrl_num_meas_low	1
Fg_ctrl_many_outliers	1
Fg_ctrl_sunclinT	1
Fg_ctrl_moonglint	1
Fg_ctrl_reach_maxiter	1
Fg_ctrl_marq	1
Fg_ctrl_chi2	1
Fg_ctrl_chi2_p	1
Fg_ctrl_gal_noise	1
Fg_ctrl_suspect_rfi	1
Fg_sc_low_wind	0
Fg_sc_land_sea_coast1	0
Fg_sc_ice	1
Fg_sc_suspect_ice	1
Fg_sc_sea_state_1	1
Fg_sc_sea_state_5	1

Full description of the flags appears in the SMOS Level 2 and Auxiliary Data Products Specifications document (see references at the end of the document). In addition, the following parameters can be controlled via threshold to retain only the best data: $Dg_af_fov > 130$. Note that these filter strategies offer the best quality results, but with a significant reduction of valid grid points. Users may consider relaxing some of the criteria to improve spatial coverage. For instance, the use of Dg_af_fov (typically spamming from 0 to 256 measurements) has the side effect of clipping the sides of the orbits, reducing the width of the track in the orbit to approximately 700 kms. By selecting the recommended criteria, users are selecting grid points that have been obtained primarily from measurements situated in the Alias-Free Field of View (AF-FOV) of the SMOS snapshots, which penalizes grid points with a larger proportion of measurements from the Extended AF-FOV (EAF-FOV).

Flags used before MDB files generation

We only select data in the MDB files such as the following conditions or flags are met:

- $Dg_af_fov > 130$
- `control_flag_set: CTRL_ECMWF`
- `control_flag_clear: CTRL_NUM_MEAS_MIN, CTRL_NUM_MEAS_LOW, CTRL_MANY_OUTLIERS, CTRL_SUNGLINT, CTRL_MOONGLINT, CTRL_REACH_MAXITER, CTRL_MARQ, CTRL_CHI2_P, CTRL_SUSPECT_RFI`
- `science_flag_set: SC_LOW_WIND, SC_LAND_SEA_COAST1`
- `science_flag_clear: SC_ICE, SC_SUSPECT_ICE`

Satellite SSS product characteristics

Table 2: Satellite SSS product characteristics

SMOS SSS L2 v700 (ESA)	
Spatial resolution	~40 km
Temporal repeat	3 days
Temporal coverage	From 2010-06-01 to now
Spatial coverage	Global [-180 180 -90 90]
Data Provider	ESA
Version	700
ATBD	SMOS_L2OS-ATBD
Data access	level-2-ocean-salinity
DOI	10.57780/SM1-294cb1b

2.2 *In situ* SSS dataset

The TSG (SAMOS) dataset corresponds to "Research" quality data from the US Shipboard Automated Meteorological and Oceanographic System (SAMOS) initiative ([Smith et al. \(2009\)](#)). Data are available at <http://samos.coaps.fsu.edu/html/>. Adjusted values when available and only collected TSG data that exhibit quality flags=1 and 2 were used. After visual inspection,

data from the NANCY FOSTER (ID="WTER", IMO="008993227") with date 2011/03/21 and all data from the ATLANTIS (ID="KAQP", IMO="009105798") for year 2010 have been removed from this dataset. For years, 2013 to 2022, RV Laurence Gould And Nathaniel Palmer data are coming from the "Intermediate" repository and have been quality controlled. The entire database has been resampled at a 10-minute time frequency data rate.

2.3 Auxiliary geophysical datasets

Additional EO datasets are used to characterize the geophysical conditions at the *in situ*/satellite SSS pair measurement locations and time, and 10 days prior to the measurements, to get an estimate of the geophysical concomitant condition and history. As discussed in [Boutin et al. \(2016\)](#), the presence of vertical gradients in, and horizontal variability of, sea surface salinity indeed complicates comparison of satellite and *in situ* measurements. The additional EO data are used here to get a first estimates of conditions for which L-band satellite SSS measured in the first centimeters of the upper ocean within a 50-150 km diameter footprint might differ from pointwise *in situ* measurements performed in general between 10 and 5 m depth below the surface. The spatio-temporal variability of SSS within a satellite footprint (50–150 km) is a major issue for satellite SSS validation in the vicinity of river plumes, frontal zones, and significant precipitation areas, among others. Rainfall can in some cases produce vertical salinity gradients exceeding 1 pss m^{-1} ; consequently, it is recommended that satellite and *in situ* SSS measurements less than 3–6 h after rain events should be considered with care when used in satellite calibration/validation analyses. To identify such situation, the Pi-MEP platform is first using [CMORPH](#) products to characterize the local value and history of rain rate and [ASCAT](#) gridded data are used to characterize the local surface wind speed and history. For validation purpose, the [ISAS](#) monthly SSS *in situ* analysed fields at 5 m depth are collocated and compared with the satellite SSS products. The use of ISAS is motivated by the fact that it is used in the SMOS L2 official validation protocol in which systematic comparisons of SMOS L2 retrieved SSS with ISAS are done. In complement to ISAS, monthly std climatological fields from the World Ocean Atlas (WOA13) at the match-up pairs location and date are also used to have an a priori information of the local SSS variability.

2.3.1 CMORPH

Precipitation are estimated using the [CMORPH](#) 3-hourly products at $1/4^\circ$ resolution ([Joyce et al. \(2004\)](#)). CMORPH (CPC MORPHing technique) produces global precipitation analyses at very high spatial and temporal resolution. This technique uses precipitation estimates that have been derived from low orbiter satellite microwave observations exclusively, and whose features are transported via spatial propagation information that is obtained entirely from geostationary satellite IR data. At present NOAA incorporate precipitation estimates derived from the passive microwaves aboard the DMSP 13, 14 and 15 (SSM/I), the NOAA-15, 16, 17 and 18 (AMSU-B), and AMSR-E and TMI aboard NASA's Aqua, TRMM and GPM spacecraft, respectively. These estimates are generated by algorithms of [Ferraro \(1997\)](#) for SSM/I, [Ferraro et al. \(2000\)](#) for AMSU-B and [Kummerow et al. \(2001\)](#) for TMI. Note that this technique is not a precipitation estimation algorithm but a means by which estimates from existing microwave rainfall algorithms can be combined. Therefore, this method is extremely flexible such that any precipitation estimates from any microwave satellite source can be incorporated.

With regard to spatial resolution, although the precipitation estimates are available on a grid with a spacing of 8 km (at the equator), the resolution of the individual satellite-derived estimates is coarser than that - more on the order of $12 \times 15 \text{ km}$ or so. The finer "resolution" is obtained via interpolation.

In effect, IR data are used as a means to transport the microwave-derived precipitation features during periods when microwave data are not available at a location. Propagation vector matrices are produced by computing spatial lag correlations on successive images of geostationary satellite IR which are then used to propagate the microwave derived precipitation estimates. This process governs the movement of the precipitation features only. At a given location, the shape and intensity of the precipitation features in the intervening half hour periods between microwave scans are determined by performing a time-weighting interpolation between microwave-derived features that have been propagated forward in time from the previous microwave observation and those that have been propagated backward in time from the following microwave scan. NOAA refer to this latter step as "morphing" of the features.

For the present Pi-MEP products, we only considered the 3-hourly products at 1/4 degree resolution. The entire CMORPH record (December 2002-present) for 3-hourly, 1/4 degree lat/lon resolution can be found at: ftp://ftp.cpc.ncep.noaa.gov/precip/CMORPH_V1.0/CRT/. CMORPH estimates cover a global belt (-180°W to 180°E) extending from 60°S to 60°N latitude and are available for the complete period of the Pi-MEP core datasets (Jan 2010-now).

2.3.2 ASCAT

Advanced SCATterometer (ASCAT) daily data produced and made available at [Ifremer/CERSAT](#) on a 0.25°x0.25° resolution grid ([Bentamy and Fillon \(2012\)](#)) since March 2007 are used to characterize the mean daily wind at the match-up pair location as well as the wind history during the 10-days period preceding the in situ measurement date. These wind fields are calculated based on a geostatistical method with external drift. Remotely sensed data from ASCAT are considered as observations while those from numerical model analysis (ECMWF) are associated with the external drift. The spatial and temporal structure functions for wind speed, zonal and meridional wind components are estimated from ASCAT retrievals. Furthermore, the new procedure includes a temporal interpolation of the retrievals based on the complex empirical orthogonal function (CEOF) approach, in order to enhance the sampling length of the scatterometer observations. The resulting daily wind fields involves the main known surface wind patterns as well as some variation modes associated with temporal and spatial moving features. The accuracy of the gridded winds was investigated through comparisons with moored buoy data in [Bentamy et al. \(2012\)](#) and resulted in rms differences for wind speed and direction are about 1.50 m.s⁻¹ and 20°.

2.3.3 ISAS

The In Situ Analysis System (ISAS), as described in [Gaillard et al. \(2016\)](#) is a data based re-analysis of temperature and salinity fields over the global ocean 70°N–70°S on a 1/2° grid. It was initially designed to synthesize the temperature and salinity profiles collected by the Argo program. It has been later extended to accommodate all type of vertical profile as well as time series. ISAS gridded fields are entirely based on *in situ* measurements. The methodology and configuration have been conceived to preserve as much as possible the data information content and resolution. ISAS is developed and run in a research laboratory ([LOPS](#)) in close collaboration with Coriolis, one of Argo Global Data Assembly Center and unique data provider for the Mercator operational oceanography system. In Pi-MEP, the products used are the [INSITU_GLO_PHY_TS_OA_MY_013.052](#) for the period 2010 to 2021 and the [INSITU_GLO_PHY_TS_OA_NRT_013.002](#) for the Near-Real Time (2022-2023) derived at the Coriolis data center and provided by the Copernicus Marine Environment Monitoring Service ([CMEMS](#)). The major contribution to the data set is from Argo array of profiling floats, reaching an approximate resolution of one profile every 10-days and every 3-degrees over the satellite SSS period

(<http://www.umr-lops.fr/SNO-Argo/Products/ISAS-T-S-fields/>). The ISAS optimal interpolation involves a structure function modeled as the sum of two Gaussian functions, each associated with specific time and space scales, resulting in a smoothing over typically 3 degrees. The smallest scale which can be retrieved with ISAS analysis is not smaller than 300–500 km (Kolodziejczyk et al. (2015)). For validation purpose, the ISAS monthly SSS fields at 5 m depth are collocated and compared with the satellite SSS products and included in the Pi-MEP Match-up files. In addition, the "percentage of variance" fields (PCTVAR) contained in the ISAS analyses provide information on the local variability of *in situ* SSS measurements within $1/2^\circ \times 1/2^\circ$ boxes.

2.3.4 World Ocean Atlas Climatology

The World Ocean Atlas (WOA) is a set of objectively analyzed (1° grid) climatological fields of *in situ* temperature, salinity and other variables provided at standard depth levels for annual, seasonal, and monthly compositing periods for the World Ocean. It also includes associated statistical fields of observed oceanographic profile data interpolated to standard depth levels on 5° , 1° , and 0.25° grids. We use these fields in complement to ISAS to characterize the climatological fields (monthly mean and std) at the match-up pairs location and date.

2.4 Overview of the Match-ups generation method

The match-up production is basically a three steps process:

1. preparation of the input *in situ* and satellite data, and,
2. co-localization of satellite products with *in situ* SSS measurements.
3. co-localization of the *in situ*/satellite pair with auxiliary information.

In the following, we successively detail the approaches taken for these different steps.

2.4.1 *In situ*/Satellite data filtering

The first step consists in filtering TSG (SAMOS) *in situ* data using the quality flags as described in 2.2 so that only valid salinity data remain in the final match-up files.

For high-spatial resolution *in situ* SSS measurements such as the Thermo-SalinoGraph (TSG) SSS data, as well as SSS data from surface drifters, an additional spatial filtering step is performed on the *in situ* data that will be eventually compared to the satellite SSS products. If R_{sat} is the spatial resolution of the satellite SSS product (L2 to L3-L4), the *in situ* data are spatially low pass filtered using a running median filter with a window width= R_{sat} to try to minimize the spatial representation uncertainty when comparing to the lower spatial resolution of the satellite SSS product. Both original and filtered *in situ* data are finally stored in the MDB files.

Only for satellite L2 SSS data, a third sub-step consists in filtering spurious data using the flags and associated recommendations as provided by the official data centers and described in 2.1.

2.4.2 *In situ*/Satellite Co-localization

In this step, each SSS satellite product is co-localized with the filtered *in situ* measurements. The method used for co-location is different if the satellite SSS is a swath product (so-called Level 2-types) or a time-space composite product (so-called Level 3/level 4-types).

- For L2 SSS swath data :

If R_{sat} is the spatial resolution of the satellite swath SSS product, for each *in situ* data sample collected in the Pi-MEP database, the platform searches for all satellite SSS data found at grid nodes located within a radius of $R_{sat}/2$ from the *in situ* data location and acquired with a time-lag from the *in situ* measurement date that is less or equal than ± 12 hours. If several satellite SSS samples are found to meet these criteria, the final satellite SSS match-up point is selected to be the closest in time from the *in situ* data measurement date. The final spatial and temporal lags between the *in situ* and satellite data are stored in the MDB files.

- For L3 and L4 composite SSS products :

If R_{sat} is the spatial resolution of the composite satellite SSS product and D the period over which the composite product was built (e.g., periods of 1, 7, 8, 9, 10, 18 days, 1 month, etc..) with central time t_o , then for each *in situ* data sample in the Pi-MEP database within the time interval $[t_o - D/2, t_o + D/2]$, the platform searches for all satellite SSS data of the composite product found at grid nodes located within a radius of $R_{sat}/2$ from the *in situ* data location. If several satellite SSS product samples are found to meet these criteria, the final satellite SSS match-up point is chosen to be the composite SSS with central time t_o which is the closest in time to the *in situ* data measurement date. The final spatial and temporal lags between the *in situ* and satellite data are stored in the MDB file.

Recently, in the context of the partnership with NASA, the Pi-MEP provides a new co-localization criterion that is applied only to L2 products, called "L2-Averaged". It consists in averaging all SSS L2 swath pixels falling in a spatio-temporal window defined by $R_{sat}=50\text{km}$ and $D = \pm 3.5$ days around the *in situ* location. The spatial and temporal lags stored in the MDB files correspond to the average of all lags for each *in situ* data.

2.4.3 MDB pair Co-localization with auxiliary data and complementary information

MDB data consist of satellite and *in situ* SSS pairs but also of auxiliary geophysical parameters such as local and history of wind speed and rain rates, as well as various information (climatology, distance to coast, mixed layer depth, barrier layer thickness, etc) that can be derived from *in situ* data and which are included in the final match-up files. The collocation of auxiliary parameters and additional information is done for each *in situ* SSS measurement contained in the match-up files as follows :

If t_{insitu} is the time/date at which the *in situ* measurement is performed, we collect:

- The [ASCAT](#) wind speed product of the same day than t_{insitu} found at the ASCAT $1/4^\circ$ grid node with closest distance from the *in situ* data location. We then store the time series of the ASCAT wind speed at the same node for the 10 days prior to the *in situ* measurement day.
- If the *in situ* data is located within the $60^\circ\text{N}-60^\circ\text{S}$ band, we select the [CMORPH](#) 3-hourly product that is closest in time from t_{insitu} and found at the CMORPH $1/4^\circ$ grid node with closest distance from the *in situ* data location. We then store the time series of the CMORPH rain rate at the same node for the 10 days prior to the *in situ* measurement time.

For the given month/year of the *in situ* data, we select the [ISAS](#) and [WOA](#) fields for the same month (and same year for ISAS fields) and take the SSS analysis (monthly mean, std) found at the closest grid node from the *in situ* measurement.

The distance from the *in situ* SSS data location to the nearest coast is evaluated and provided in km. We use a distance-to-coast map at $1/4^\circ$ resolution where small islands have been removed.

When vertical profiles of salinity (S) and temperature (T) are made available from the *in situ* measurements used to build the match-up (Argo or marine mammals), the following variables are also included into each satellite/*in situ* match-up file:

1. The vertical distribution of pressure at which the profiles were measured,
2. The vertical $S(z)$ and $T(z)$ profiles,
3. The vertical potential density anomaly profile $\sigma_0(z)$,
4. The Mixed Layer Depth (MLD). The MLD is defined here as the depth where the potential density has increased from the reference depth (10 meter) by a threshold equivalent to 0.2°C decrease in temperature at constant salinity: $\sigma_0 = \sigma_{010m} + \Delta\sigma_0$ with $\Delta\sigma_0 = \sigma_0(\theta_{10m} - 0.2, S_{10m}) - \sigma_0(\theta_{10m}, S_{10m})$ where θ_{10m} and S_{10m} are the temperature and salinity at the reference depth (i.e. 10 m) (de Boyer Montégut et al. (2004), de Boyer Montégut et al. (2007)).
5. The Top of the Thermocline Depth (TTD) is defined as the depth at which temperature decreases from its 10 m value by 0.2°C .
6. The Barrier Layer thickness (BLT) is defined as the difference between the MLD and the TTD. If $\text{BLT} < 0$, it corresponds to a vertically density compensated layer whose thickness is then the absolute value of (TTD-MLD).
7. The vertical profile of the buoyancy frequency $N^2(z)$

The resulting match-ups files are serialized as NetCDF-4 files whose structure depends on the origin of the *in situ* data and is described in section 2.4.4.

2.4.4 Content of the Match-Up NetCDF files

The content of the Match-Up NetCDF files for TSG (SAMOS) is described [here](#).

2.5 MDB characteristics for each specific *in situ*/satellite pair

2.5.1 Number of paired SSS data as a function of time and distance to coast

Figure 2 shows the time (a) and distance to coast (b) distributions of the match-ups between TSG (SAMOS) and SMOS SSS L2 v700 (ESA) for the SPURS 2 Pi-MEP region and for the full satellite product period.

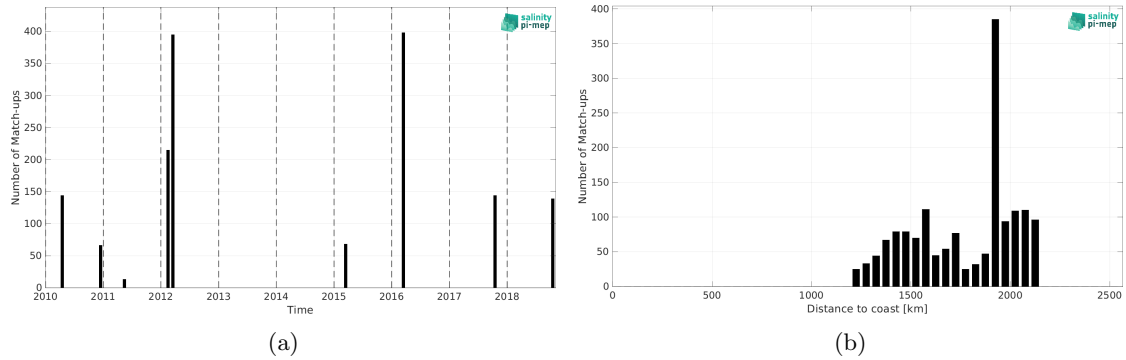


Figure 2: Number of match-ups between TSG (SAMOS) and SMOS SSS L2 v700 (ESA) SSS as a function of time (a) and as function of the distance to coast (b) over the SPURS 2 Pi-MEP region and for the full satellite product period.

2.5.2 Histograms of the SSS match-ups

Figure 3 shows the SSS distribution of TSG (SAMOS) (a) and SMOS SSS L2 v700 (ESA) (b) considering all match-up pairs per bins of 0.1 over the SPURS 2 Pi-MEP region and for the full satellite product period.

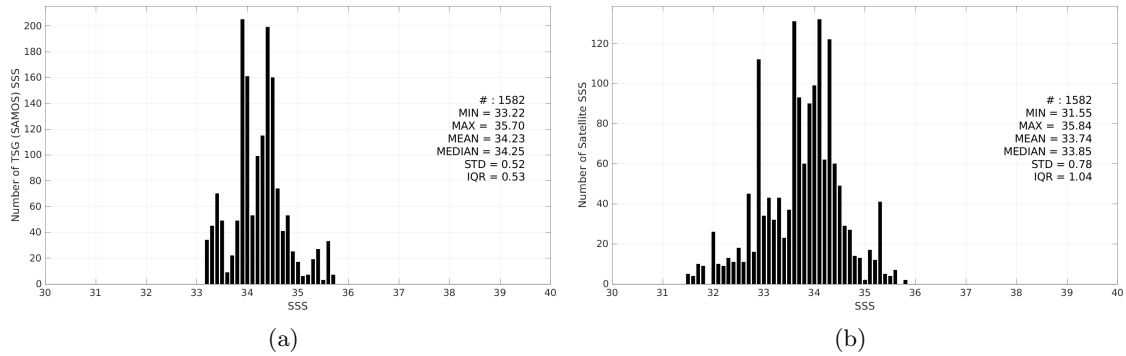


Figure 3: Histograms of SSS from TSG (SAMOS) (a) and SMOS SSS L2 v700 (ESA) (b) considering all match-up pairs per bins of 0.1 over the SPURS 2 Pi-MEP region and for the full satellite product period.

2.5.3 Distribution of *in situ* SSS depth measurements

Figure 4 shows the depth distribution of the upper level SSS measurements from TSG (SAMOS) in the Match-up DataBase for the SPURS 2 Pi-MEP region (a) and temporal mean spatial distribution of pressure of the *in situ* SSS data over $1^\circ \times 1^\circ$ boxes and for the full satellite product period (b).

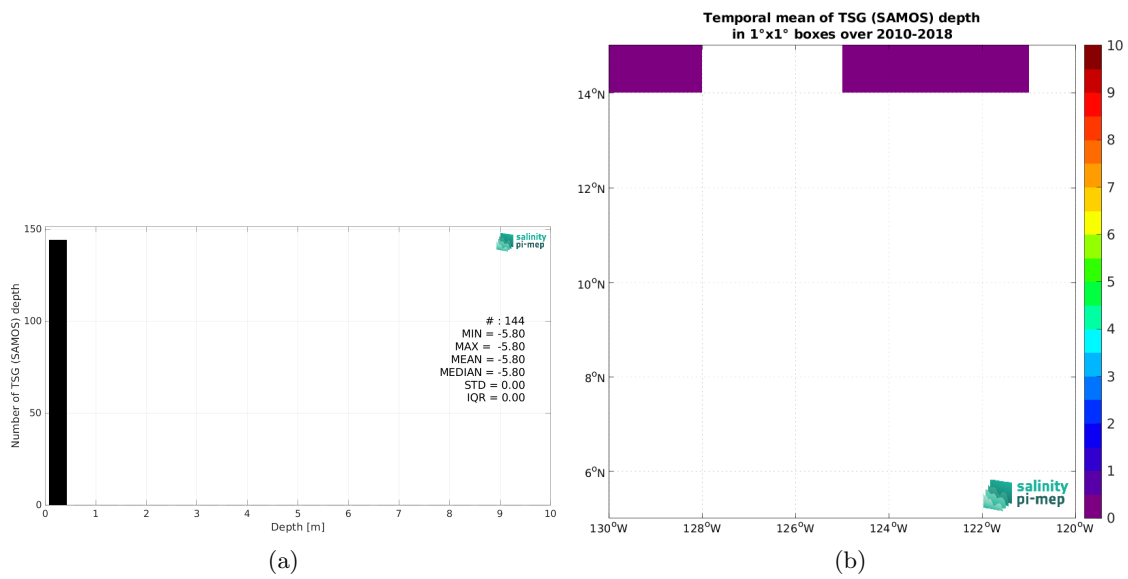


Figure 4: Histograms of the depth of the upper level SSS measurements from TSG (SAMOS) in the Match-up DataBase for the SPURS 2 Pi-MEP region (a) and temporal mean spatial distribution of pressure of the *in situ* SSS data over $1^\circ \times 1^\circ$ boxes and for the full satellite product period (b).

2.5.4 Spatial Distribution of Match-ups

The number of SSS match-ups between TSG (SAMOS) SSS and the SMOS SSS L2 v700 (ESA) SSS product for the SPURS 2 Pi-MEP region over $1^\circ \times 1^\circ$ boxes and for the full satellite product period is shown in Figure 5.

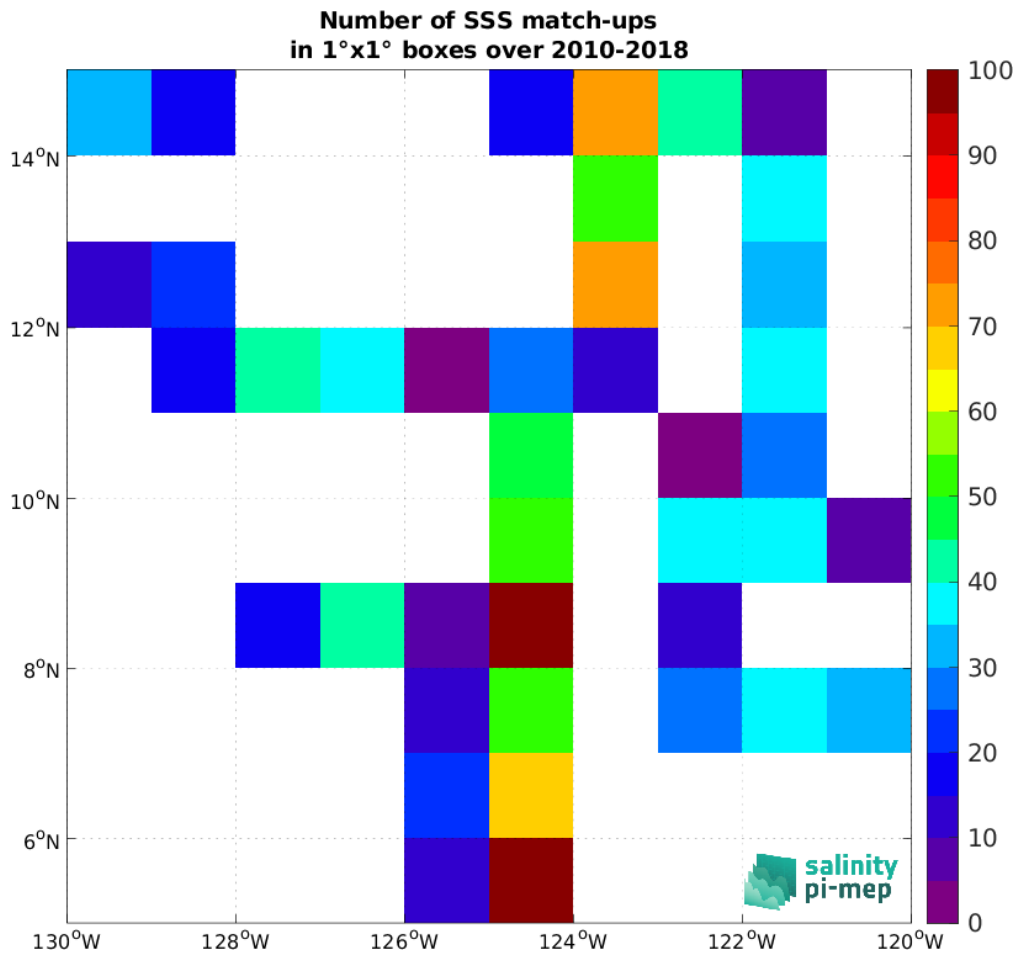


Figure 5: Number of SSS match-ups between TSG (SAMOS) SSS and the SMOS SSS L2 v700 (ESA) SSS product for the SPURS 2 Pi-MEP region over 1°x1° boxes and for the full satellite product period.

2.5.5 Histograms of the spatial and temporal lags of the match-ups pairs

Figure 6 reveals the spatial (left) and temporal (right) lags between the location/time of the TSG (SAMOS) measurement and the position/date of the corresponding SMOS SSS L2 v700 (ESA) SSS pixel of all match-ups pairs.

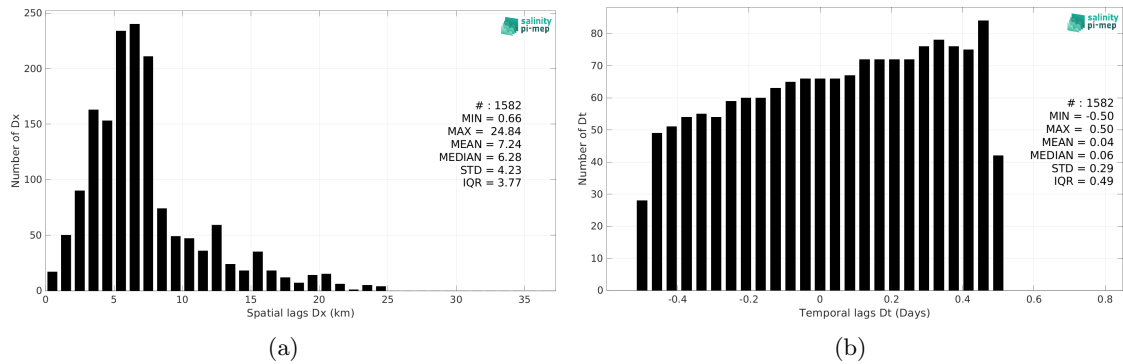


Figure 6: Histograms of the spatial (a) and temporal (b) lags between the location/time of the TSG (SAMOS) measurement and the date of the corresponding SMOS SSS L2 v700 (ESA) SSS pixel.

3 MDB file Analyses

3.1 Spatial Maps of the Temporal mean and Std of *in situ* and satellite SSS and of their difference (Δ SSS)

In Figure 7, we show maps of temporal mean (left) and standard deviation (right) of the SMOS SSS L2 v700 (ESA) (top) and of the TSG (SAMOS) *in situ* dataset at the collected Pi-MEP match-up pairs. The temporal mean and std are gridded over the full satellite product period and over spatial boxes of size $1^\circ \times 1^\circ$.

At the bottom of Figure 7, the temporal mean (left) and standard deviation (right) of the differences between the satellite SSS product and *in situ* data found at match-up pairs, namely Δ SSS(Satellite -TSG (SAMOS)), is also gridded over the full satellite product period and over spatial boxes of size $1^\circ \times 1^\circ$.

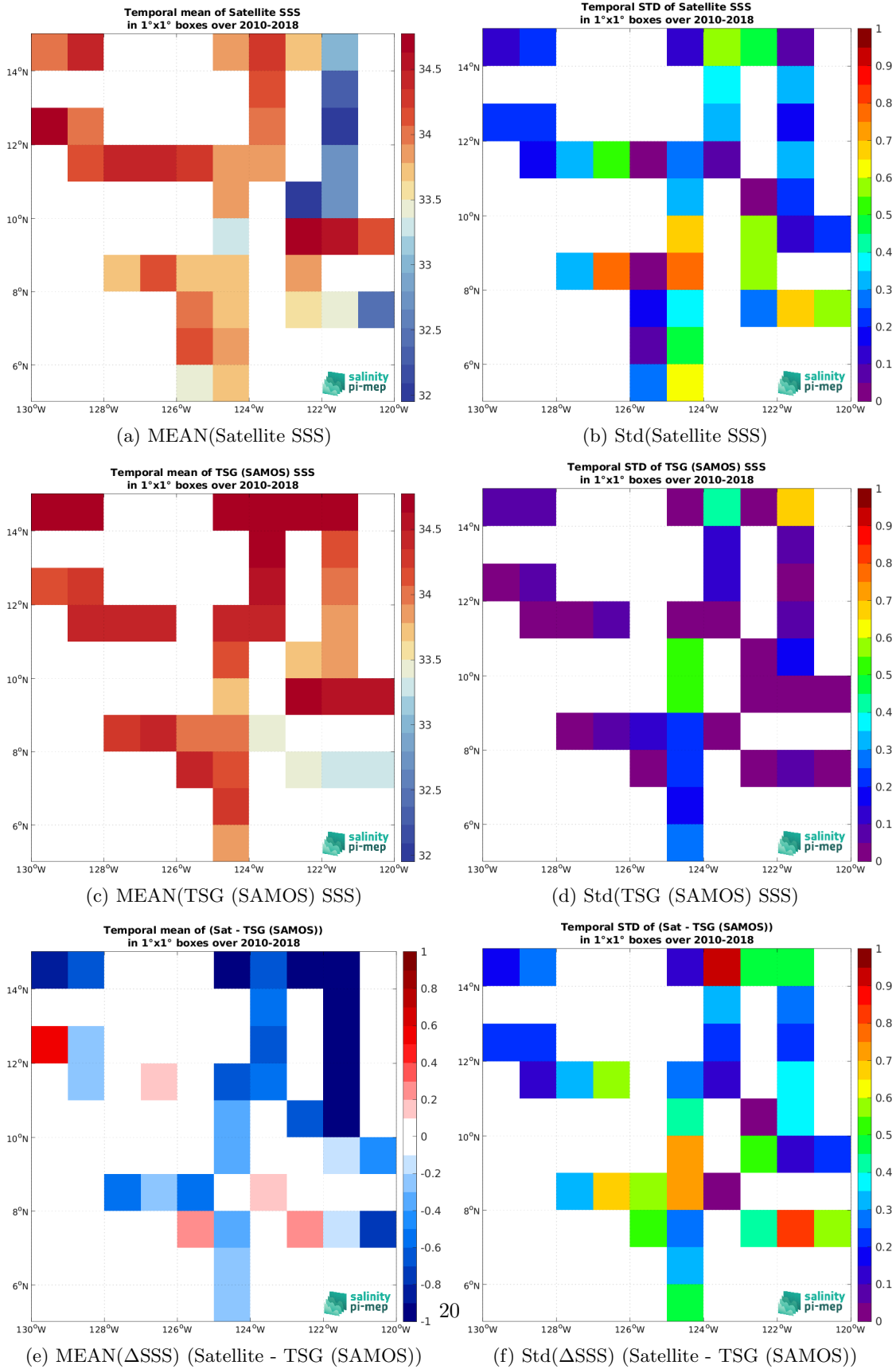


Figure 7: Temporal mean (left) and Std (right) of SSS from SMOS SSS L2 v700 (ESA) (top), TSG (SAMOS) (middle), and of Δ SSS (Satellite - TSG (SAMOS)). Only match-up pairs are used to generate these maps.

3.2 Time series of the monthly median and Std of *in situ* and satellite SSS and of their difference (Δ SSS)

In the top panel of Figure 8, we show the time series of the monthly median SSS estimated over the full SPURS 2 Pi-MEP region for both SMOS SSS L2 v700 (ESA) satellite SSS product (in black) and the TSG (SAMOS) *in situ* dataset (in blue) at the collected Pi-MEP match-up pairs.

In the middle panel of Figure 8, we show the time series of the monthly median of Δ SSS (Satellite - TSG (SAMOS)) for the collected Pi-MEP match-up pairs and estimated over the full SPURS 2 Pi-MEP region.

In the bottom panel of Figure 8, we show the time series of the monthly standard deviation of Δ SSS (Satellite - TSG (SAMOS)) for the collected Pi-MEP match-up pairs and estimated over the full SPURS 2 Pi-MEP region.

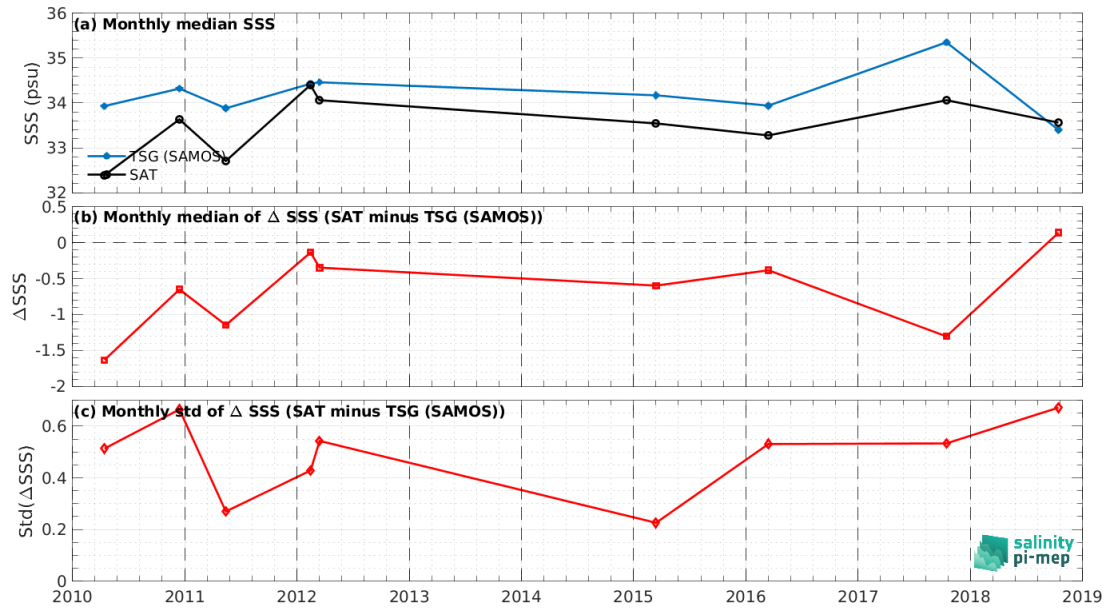


Figure 8: Time series of the monthly median SSS (top), median of Δ SSS (Satellite - TSG (SAMOS)) and Std of Δ SSS (Satellite - TSG (SAMOS)) over the SPURS 2 Pi-MEP region considering all match-ups collected by the Pi-MEP.

3.3 Zonal mean and Std of *in situ* and satellite SSS and of the difference (Δ SSS)

In Figure 9 left panel, we show the zonal mean SSS considering all Pi-MEP match-up pairs for both SMOS SSS L2 v700 (ESA) satellite SSS product (in black) and the TSG (SAMOS) *in situ* dataset (in blue). The full satellite SSS product period is used to derive the mean.

In the right panel of Figure 9, we show the zonal mean of Δ SSS (Satellite - TSG (SAMOS)) for all the collected Pi-MEP match-up pairs estimated over the full satellite product period.

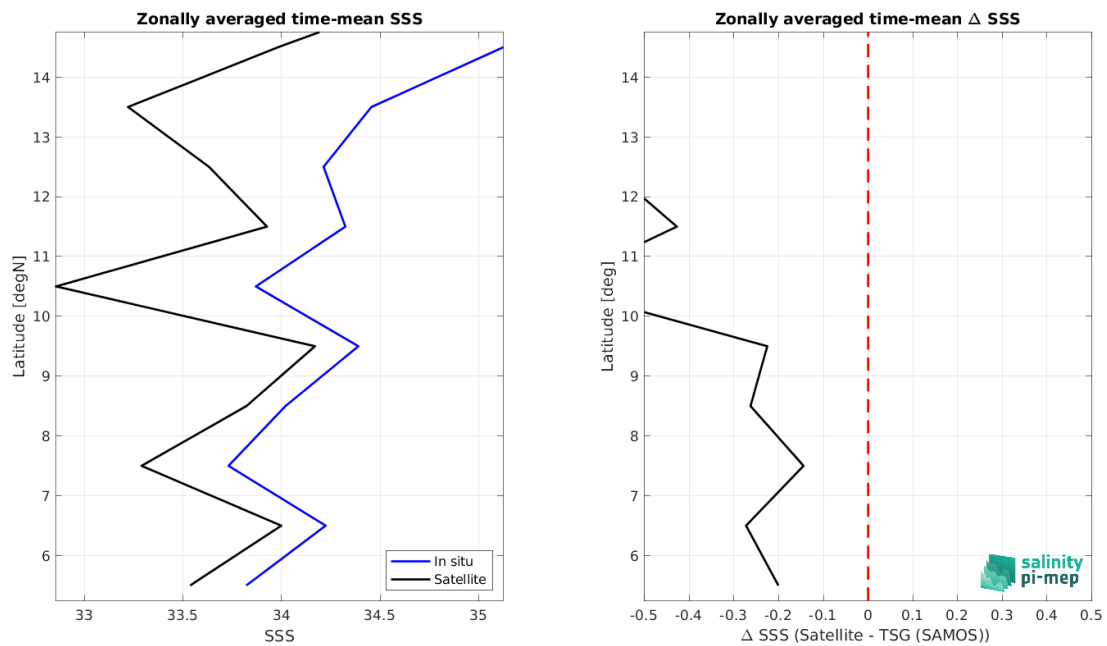


Figure 9: Left panel: Zonal mean SSS from SMOS SSS L2 v700 (ESA) satellite product (black) and from TSG (SAMOS) (blue). Right panel: Zonal mean of Δ SSS (Satellite - TSG (SAMOS)) for all the collected Pi-MEP match-up pairs estimated over the full satellite product period.

3.4 Scatterplots of satellite vs *in situ* SSS by latitudinal bands

In Figure 10, contour maps of the concentration of SMOS SSS L2 v700 (ESA) SSS (y-axis) versus TSG (SAMOS) SSS (x-axis) at match-up pairs for different latitude bands: (a) 80°S-80°N, (b) 20°S-20°N, (c) 40°S-20°S and 20°N-40°N and (d) 60°S-40°S and 40°N-60°N. For each plot, the red line shows $x=y$. The black thin and dashed lines indicate a linear fit through the data cloud and the $\pm 95\%$ confidence levels, respectively. The number match-up pairs n , the slope and R^2 coefficient of the linear fit, the root mean square (RMS) and the mean bias between satellite and *in situ* data are indicated for each latitude band in each plots.

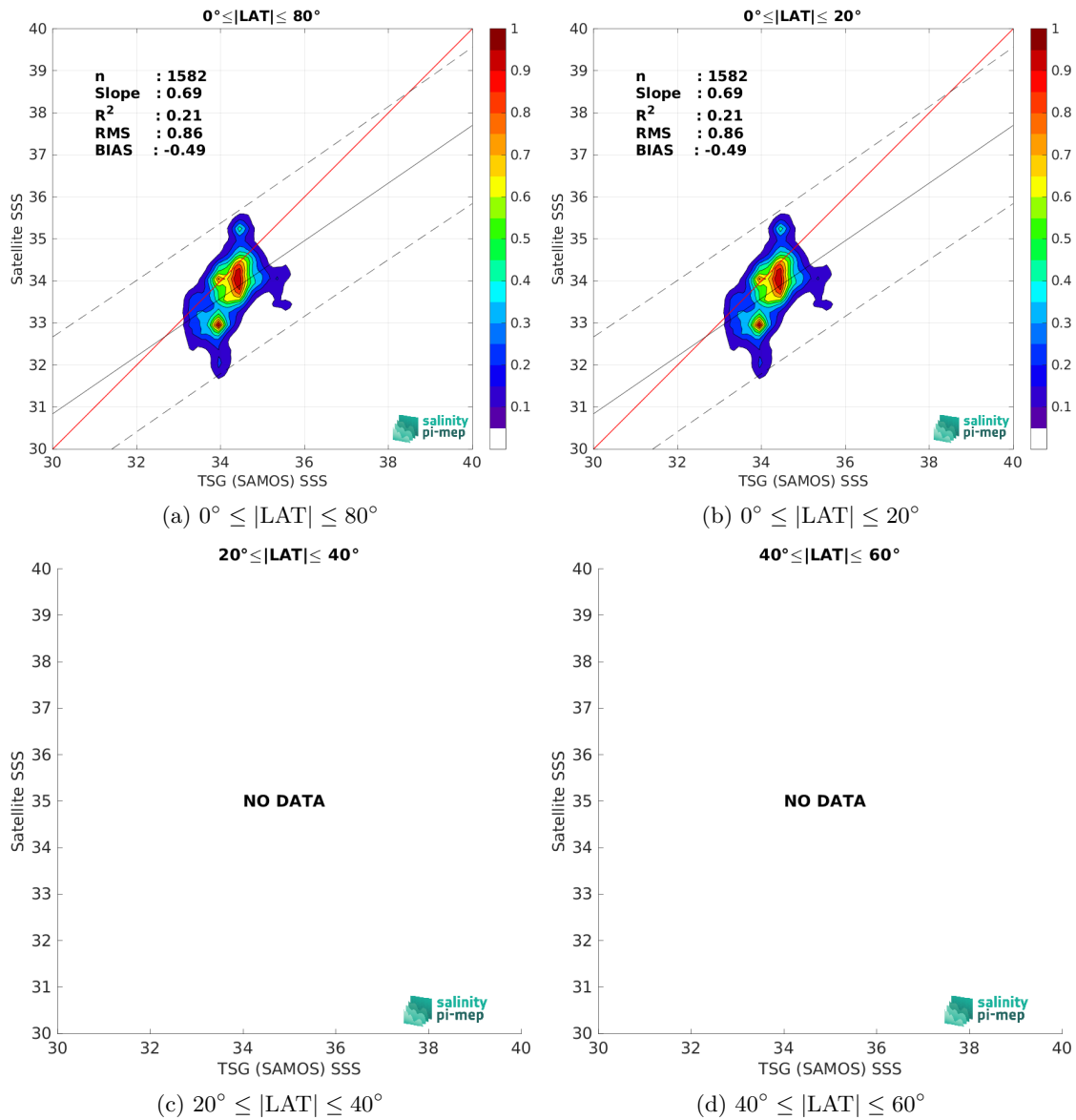


Figure 10: Contour maps of the concentration of SMOS SSS L2 v700 (ESA) SSS (y-axis) versus TSG (SAMOS) SSS (x-axis) at match-up pairs for different latitude bands. For each plot, the red line shows $x=y$. The black thin and dashed lines indicate a linear fit through the data cloud and the $\pm 95\%$ confidence levels, respectively. The number match-up pairs n , the slope and R^2 coefficient of the linear fit, the root mean square (RMS) and the mean bias between satellite and *in situ* data are indicated for each latitude band in each plots.

3.5 Time series of the monthly median and Std of ΔSSS sorted by latitudinal bands

In Figure 11, time series of the monthly median (red curves) of ΔSSS (Satellite - TSG (SAMOS)) and ± 1 Std (black vertical thick bars) as function of time for all the collected Pi-MEP match-up

pairs estimated over the SPURS 2 Pi-MEP region and for the full satellite product period are shown for different latitude bands: (a) 80°S-80°N, (b) 20°S-20°N, (c) 40°S-20°S and 20°N-40°N and (d) 60°S-40°S and 40°N-60°N.

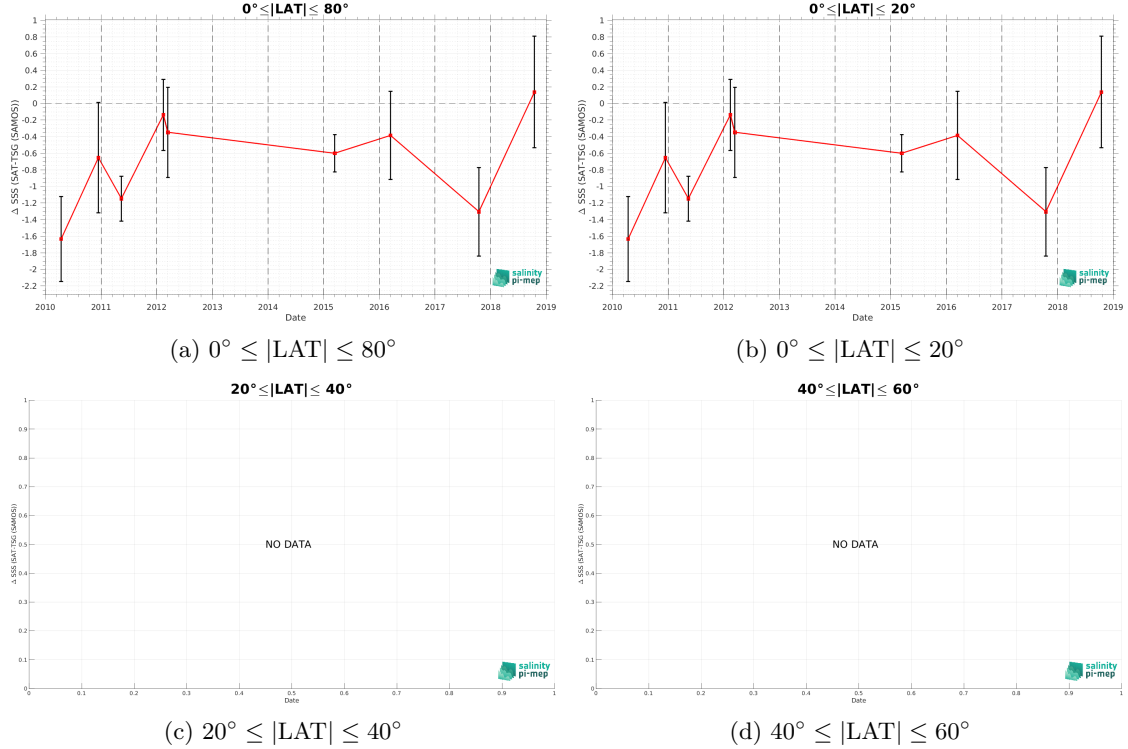


Figure 11: Monthly median (red curves) of ΔSSS (Satellite - TSG (SAMOS)) and ± 1 Std (black vertical thick bars) as function of time for all the collected Pi-MEP match-up pairs estimated over the SPURS 2 Pi-MEP region and for the full satellite product period are shown for different latitude bands: (a) 80°S-80°N, (b) 20°S-20°N, (c) 40°S-20°S and 20°N-40°N and (d) 60°S-40°S and 40°N-60°N.

3.6 ΔSSS sorted as function of geophysical parameters

In Figures 12 and 13, we classify the match-up differences ΔSSS (Satellite - *in situ*) between SMOS SSS L2 v700 (ESA) and TSG (SAMOS) SSS as function of the geophysical conditions at match-up points. The median and std of ΔSSS (Satellite - TSG (SAMOS)) is thus evaluated as function of the

- *in situ* SSS values per bins of width 0.2,
- *in situ* SST values per bins of width 1°C,
- CCMP 6h/ASCAT daily wind values per bins of width 1 m/s,
- IMERG 30 min/CMORPH 3-hourly rain rates per bins of width 1 mm/h,
- distance to the coast per bins of width 50 km,
- distance to the ice edge per bins of width 50 km,

- *in situ* measurement depth (if relevant),
- sea ice fraction per bins of width 10%,
- CMC/ERA5/AVHRR SST values per bins of width 1°C,
- ISAS SSS values per bins of width 0.2.

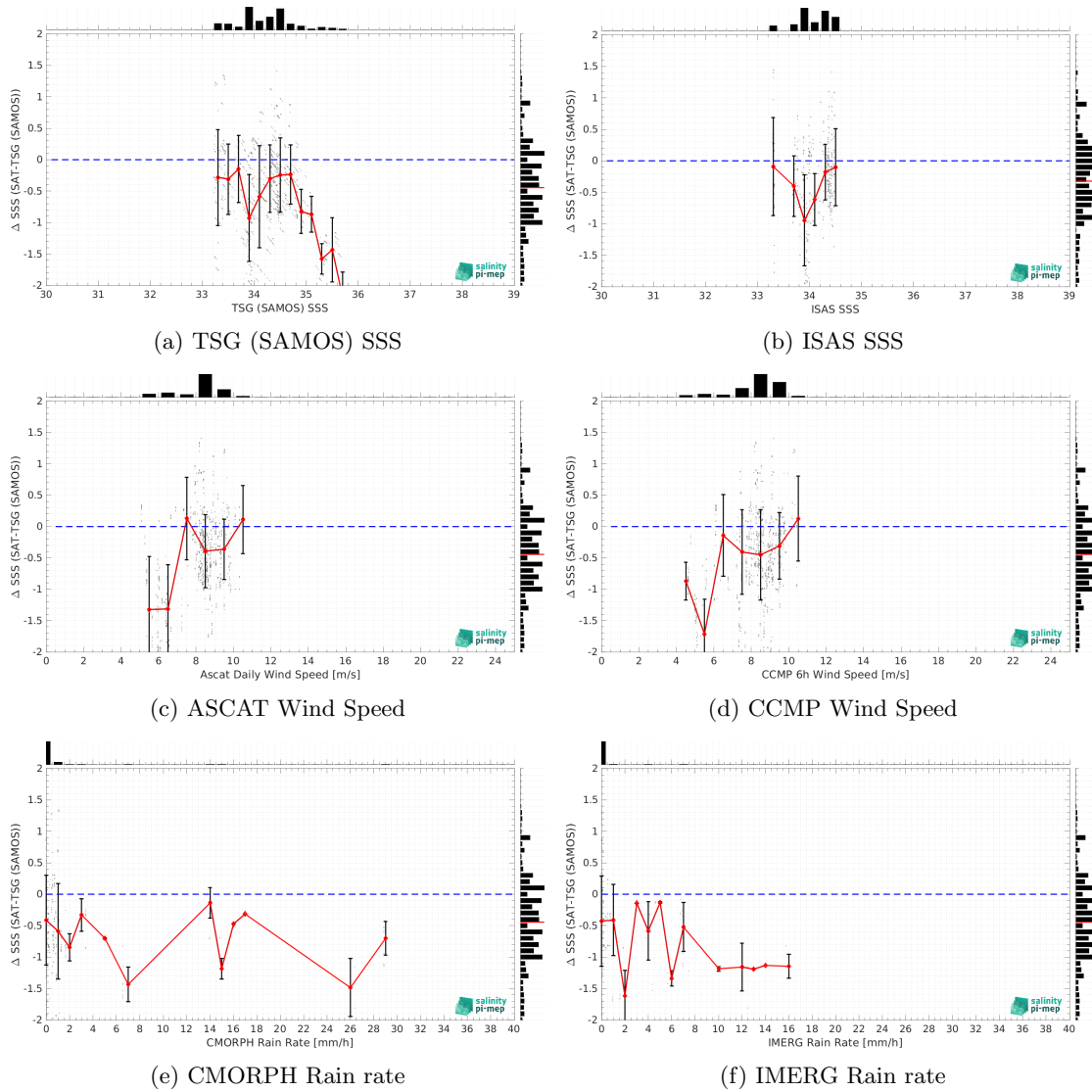


Figure 12: Δ SSS (Satellite - TSG (SAMOS)) sorted as function of TSG (SAMOS) SSS values (a), ISAS SSS (b), ASCAT Wind speed (c), CCMP Wind speed (d), CMORPH rain rate (e) and IMERG rain rate (f). In all plots the median and Std of Δ SSS for each bin is indicated by the red curves and black vertical thick bars (± 1 Std).

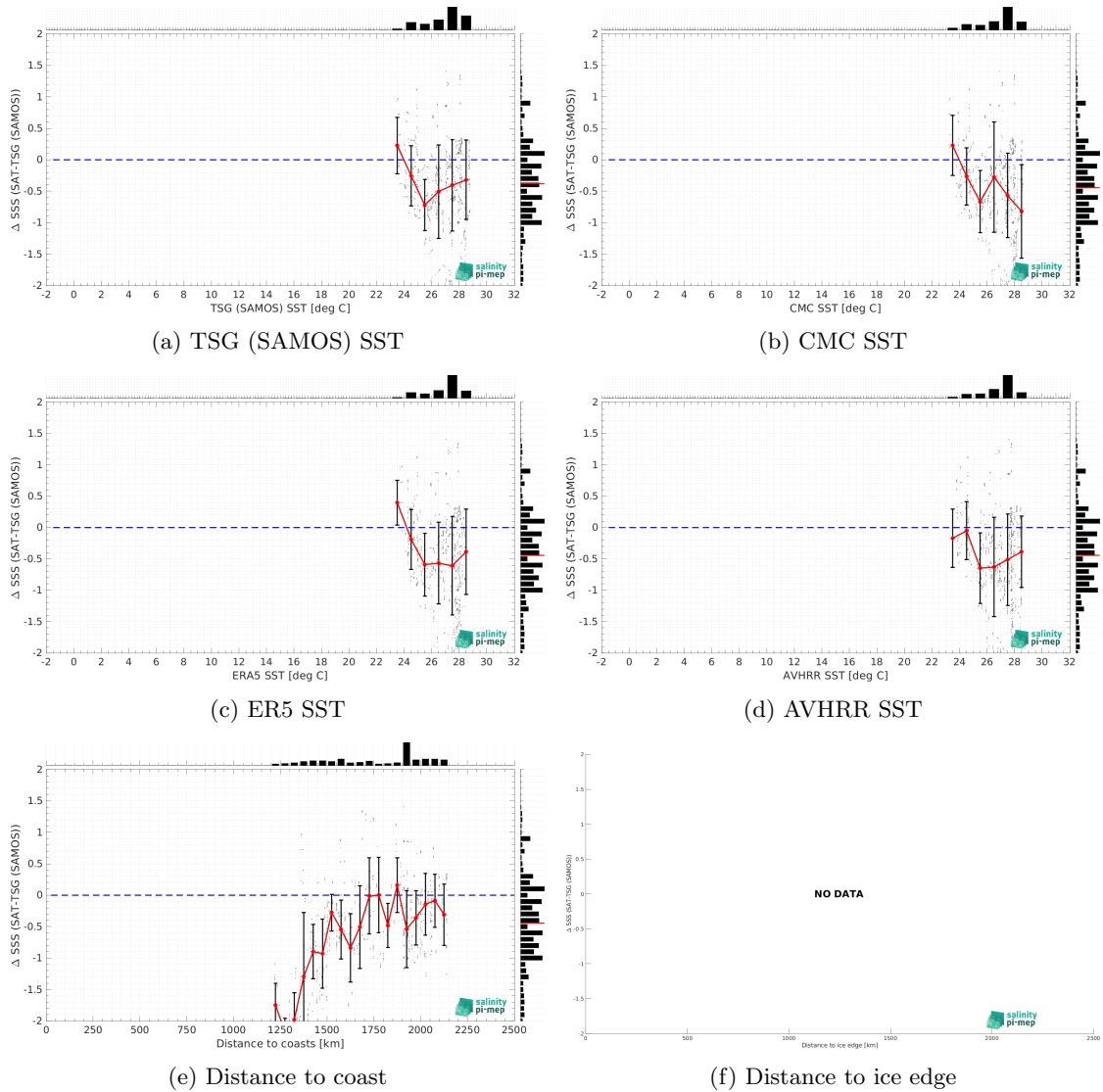


Figure 13: Δ SSS (Satellite - TSG (SAMOS)) sorted as function of TSG (SAMOS) SST values (a), CMC SST (b), ERA5 SST (c), AVHRR SST (d), distance to coast (e) and distance to ice edge (f). In all plots the median and Std of Δ SSS for each bin is indicated by the red curves and black vertical thick bars (± 1 Std). Links to similar figures sorted as function of [Sea ice fraction](#) and [in situ measurement depth](#).

3.7 Δ SSS maps and statistics for different geophysical conditions

In Figures 14 and 15, we focus on sub-datasets of the match-up differences Δ SSS (Satellite - *in situ*) between SMOS SSS L2 v700 (ESA) and TSG (SAMOS) for the following specific geophysical conditions:

- **C1:** if the local value at *in situ* location of estimated rain rate is zero, mean daily wind is in the range [3, 12] m/s, the SST is $> 5^\circ\text{C}$ and distance to coast is > 800 km.

- **C2**:if the local value at *in situ* location of estimated rain rate is zero, mean daily wind is in the range [3, 12] m/s.
- **C3**:if the local value at *in situ* location of estimated rain rate is high (ie. > 1 mm/h) and mean daily wind is low (ie. < 4 m/s).
- **C5**:if the *in situ* data is located where the climatological SSS standard deviation is low (ie. above < 0.2).
- **C6**:if the *in situ* data is located where the climatological SSS standard deviation is high (ie. above > 0.2).

For each of these conditions, the temporal mean (gridded over spatial boxes of size $1^\circ \times 1^\circ$) and the histogram of the difference ΔSSS (Satellite - *in situ*) are presented.

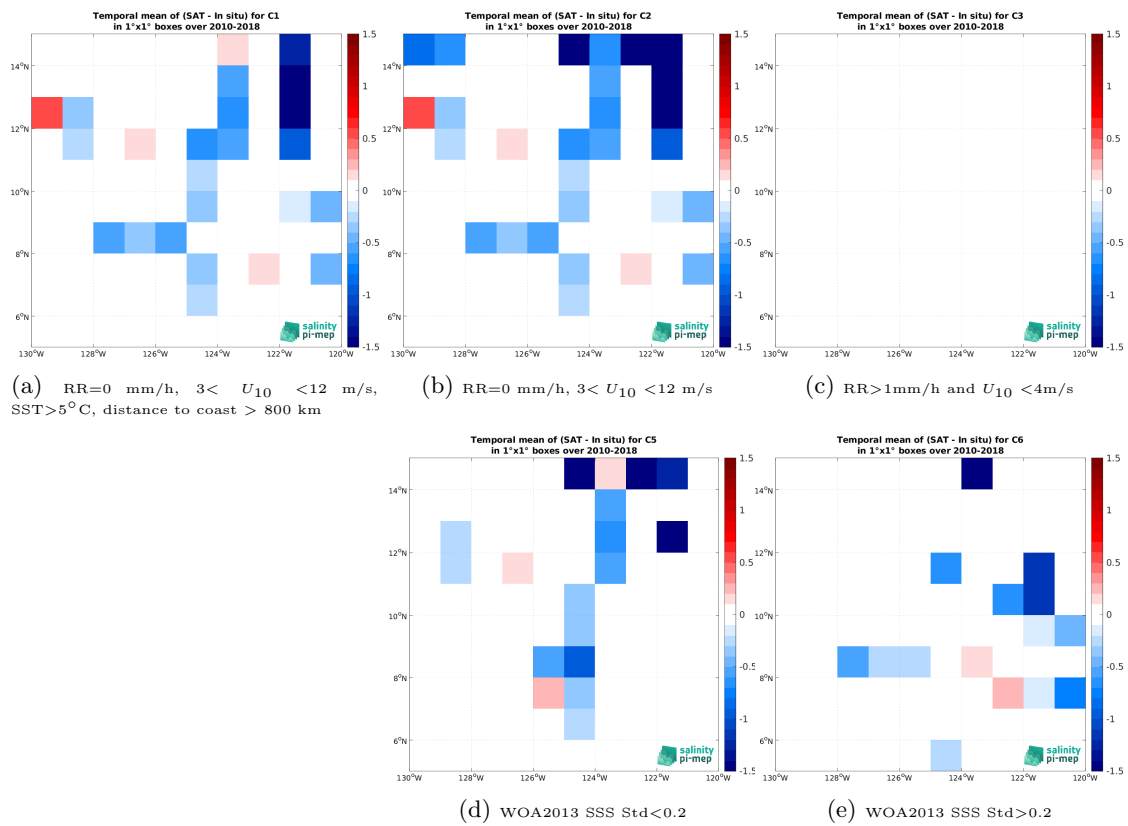


Figure 14: Temporal mean gridded over spatial boxes of size $1^\circ \times 1^\circ$ of ΔSSS (SMOS SSS L2 v700 (ESA) - TSG (SAMOS)) for 5 different subdatasets corresponding to:RR=0 mm/h, $3 < U_{10} < 12$ m/s, SST $>5^\circ\text{C}$, distance to coast > 800 km (a), RR=0 mm/h, $3 < U_{10} < 12$ m/s (b), RR >1 mm/h and $U_{10} < 4$ m/s (c), WOA2013 SSS Std <0.2 (d), WOA2013 SSS Std >0.2 (e).

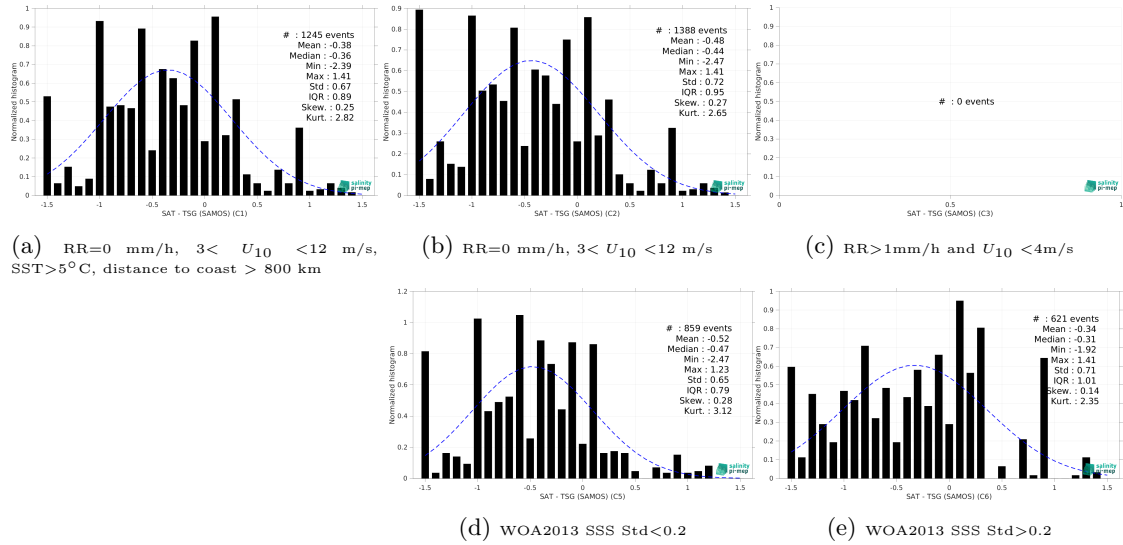


Figure 15: Normalized histogram of Δ SSS (SMOS SSS L2 v700 (ESA) - TSG (SAMOS)) for 5 different subdatasets corresponding to: RR=0 mm/h, $3 < U_{10} < 12$ m/s, SST > 5°C, distance to coast > 800 km (a), RR=0 mm/h, $3 < U_{10} < 12$ m/s (b), RR > 1mm/h and $U_{10} < 4$ m/s (c), WOA2013 SSS Std < 0.2 (d), WOA2013 SSS Std > 0.2 (e).

4 Summary

► Table 1 shows the mean, median, standard deviation (Std), root mean square (RMS), interquartile range (IQR), correlation coefficient (r^2) and robust standard deviation (Std*) of the match-up differences Δ SSS (Satellite - *in situ*) between SMOS SSS L2 v700 (ESA) and TSG (SAMOS) derived over the SPURS 2 Pi-MEP region and for the full satellite product period and for the following conditions:

- all: All the match-up pairs satellite/*in situ* SSS values are used to derive the statistics
- C1: only pairs where RR=0 mm/h, $3 < U_{10} < 12$ m/s, SST > 5°C, distance to coast > 800 km
- C2: only pairs where RR=0 mm/h, $3 < U_{10} < 12$ m/s
- C3: only pairs where RR > 1mm/h and $U_{10} < 4$ m/s
- C5: only pairs where WOA2013 SSS Std < 0.2
- C6: only pairs at WOA2013 SSS Std > 0.2
- C7a: only pairs with a distance to coast < 150 km.
- C7b: only pairs with a distance to coast in the range [150, 800] km.
- C7c: only pairs with a distance to coast > 800 km.
- C8a: only pairs where SST is < 5°C.
- C8b: only pairs where SST is in the range [5, 15]°C.

- C8c: only pairs where SST is $> 15^{\circ}\text{C}$.
- C9a: only pairs where SSS is < 33 .
- C9b: only pairs where SSS is in the range $[33, 37]$.
- C9c: only pairs where SSS is > 37 .

Table 1: Statistics of ΔSSS (Satellite - TSG (SAMOS))

Condition	#	Median	Mean	Std	RMS	IQR	r^2	Std*
all	1582	-0.44	-0.49	0.71	0.86	0.94	0.206	0.72
C1	1245	-0.36	-0.38	0.67	0.77	0.89	0.274	0.67
C2	1388	-0.44	-0.48	0.72	0.86	0.95	0.162	0.73
C3	0	NaN	NaN	NaN	NaN	NaN	NaN	NaN
C5	859	-0.47	-0.52	0.65	0.83	0.79	0.173	0.57
C6	621	-0.31	-0.34	0.71	0.79	1.01	0.300	0.76
C7a	0	NaN	NaN	NaN	NaN	NaN	NaN	NaN
C7b	0	NaN	NaN	NaN	NaN	NaN	NaN	NaN
C7c	1582	-0.44	-0.49	0.71	0.86	0.94	0.206	0.72
C8a	0	NaN	NaN	NaN	NaN	NaN	NaN	NaN
C8b	0	NaN	NaN	NaN	NaN	NaN	NaN	NaN
C8c	1438	-0.38	-0.40	0.67	0.78	0.89	0.315	0.66
C9a	0	NaN	NaN	NaN	NaN	NaN	NaN	NaN
C9b	1582	-0.44	-0.49	0.71	0.86	0.94	0.206	0.72
C9c	0	NaN	NaN	NaN	NaN	NaN	NaN	NaN

► Table 2 presents statistics of ΔSSS (Satellite - ISAS) using only ISAS SSS values with $\text{PCTVAR} < 80\%$.

Table 2: Statistics of ΔSSS (Satellite - ISAS)

Condition	#	Median	Mean	Std	RMS	IQR	r^2	Std*
all	1582	-0.32	-0.34	0.66	0.74	0.82	0.310	0.62
C1	1245	-0.33	-0.34	0.66	0.74	0.81	0.312	0.60
C2	1388	-0.29	-0.31	0.64	0.71	0.78	0.291	0.58
C3	0	NaN	NaN	NaN	NaN	NaN	NaN	NaN
C5	859	-0.38	-0.39	0.58	0.69	0.68	0.378	0.47
C6	621	-0.18	-0.26	0.69	0.74	0.98	0.332	0.69
C7a	0	NaN	NaN	NaN	NaN	NaN	NaN	NaN
C7b	0	NaN	NaN	NaN	NaN	NaN	NaN	NaN
C7c	1582	-0.32	-0.34	0.66	0.74	0.82	0.310	0.62
C8a	0	NaN	NaN	NaN	NaN	NaN	NaN	NaN
C8b	0	NaN	NaN	NaN	NaN	NaN	NaN	NaN
C8c	1438	-0.37	-0.37	0.67	0.77	0.84	0.328	0.64
C9a	0	NaN	NaN	NaN	NaN	NaN	NaN	NaN
C9b	1582	-0.32	-0.34	0.66	0.74	0.82	0.310	0.62
C9c	0	NaN	NaN	NaN	NaN	NaN	NaN	NaN

► Numerical values can be downloaded as csv files for [Table 1](#) and [Table 2](#).

5 More Comparison/Validation Materials

5.1 Comparisons with other satellite products

► Table 1 shows the mean, median, standard deviation (Std), root mean square (RMS), interquartile range (IQR), correlation coefficient (r^2) and robust standard deviation (Std*) of the match-up differences Δ SSS (Satellite - TSG (SAMOS)) between different satellite products and **TSG (SAMOS)** derived over the SPURS 2 Pi-MEP region considering all match-up pairs satellite/*in situ* SSS values to derive the statistics:

Table 1: Statistics of Δ SSS (Satellite - TSG (SAMOS)) - All

Satellite products	#	Median	Mean	Std	RMS	IQR	r^2	Std*
smos-l2-v700	1582	-0.44	-0.49	0.71	0.86	0.94	0.206	0.72
smap-l2-rss-v6	835	-0.01	-0.20	0.64	0.67	0.58	0.328	0.43
smap-l2-rss-v6-40km	725	-0.33	-0.26	0.83	0.87	1.01	0.042	0.75
smap-l2-jpl-v5.0	852	0.05	-0.16	0.78	0.80	0.88	0.071	0.61
aquarius-l2-or-v5	206	-0.17	-0.10	0.21	0.23	0.25	0.355	0.20
aquarius-l2-jpl-v5	214	-0.05	0.03	0.26	0.27	0.31	0.318	0.27
smos-l3-catds-cpdc-v333-l2q	1158	-0.23	-0.22	0.74	0.77	0.91	0.182	0.70
smos-l3-catds-cpdc-v332-9d	2739	-0.09	-0.18	0.47	0.50	0.48	0.325	0.36
smos-l3-catds-cpdc-v335-10d-25km	2739	-0.09	-0.20	0.49	0.53	0.60	0.261	0.41
smos-l3-catds-cpdc-v335-1m-25km	2739	-0.07	-0.15	0.48	0.51	0.33	0.277	0.24
smos-l3-catds-locean-v9-9d	3901	-0.10	-0.19	0.46	0.50	0.50	0.332	0.36
smos-l3-catds-locean-v9-18d	3901	-0.12	-0.19	0.46	0.50	0.40	0.325	0.30
smos-l3-bec-v2-9d	1718	0.03	-0.04	0.57	0.58	0.78	0.175	0.58
smap-l3-rss-v6-8dr	1452	-0.02	-0.37	0.64	0.74	1.05	0.543	0.24
smap-l3-rss-v6-1m	1452	-0.14	-0.40	0.66	0.77	1.00	0.355	0.53
smap-l3-jpl-v5.0-8dr	1452	-0.02	-0.29	0.64	0.70	1.08	0.558	0.35
smap-l3-jpl-v5.0-1m	800	0.04	-0.27	0.72	0.77	1.13	0.301	0.55
aquarius-l3-or-v5-7dr	532	-0.04	0.03	0.24	0.24	0.22	0.863	0.16
aquarius-l3-or-v5-1m	532	-0.04	0.04	0.27	0.27	0.25	0.797	0.18
aquarius-l3-or-v5-7dr-rain-mask	480	-0.04	0.02	0.25	0.25	0.23	0.868	0.16
aquarius-l3-or-v5-1m-rain-mask	532	-0.01	0.06	0.26	0.26	0.23	0.820	0.17
aquarius-l3-jpl-v5-7dr	532	0.11	0.13	0.25	0.28	0.32	0.752	0.22
aquarius-l3-jpl-v5-1m	532	0.11	0.19	0.23	0.30	0.27	0.814	0.19
smos-l4-bec-v2-1d	2403	0.08	-0.02	0.55	0.55	0.71	0.222	0.53
smos-l4-cmems-catds-lops-oi-v346-1w	2352	-0.06	-0.17	0.50	0.53	0.45	0.293	0.32
smos-l4-cmems-cnr-v1-1d	2388	-0.10	-0.24	0.57	0.62	0.35	0.104	0.26
smos-l4-cmems-cnr-v1-1m	2388	-0.07	-0.20	0.53	0.57	0.34	0.183	0.25
cci-l4-esa-merged-oi-v4.41-7dr	2170	-0.11	-0.18	0.44	0.48	0.37	0.425	0.28
cci-l4-esa-merged-oi-v4.41-30dr	2174	-0.10	-0.19	0.47	0.51	0.36	0.333	0.28
smap-l4-esr-oi-v3-1d	6224	0.05	-0.14	0.59	0.60	0.46	0.212	0.33
smap-l4-esr-oi-v3-1m	1556	-0.01	-0.16	0.59	0.61	0.36	0.207	0.27
aquarius-l4-iprc-v5-1w	627	-0.13	-0.05	0.23	0.24	0.21	0.818	0.13
aquarius-l4-iprc-v5-1m	627	-0.09	-0.04	0.21	0.22	0.17	0.889	0.13
cci-l4-esa-merged-oi-v5.5-7dr	2190	-0.11	-0.15	0.44	0.47	0.32	0.424	0.23
cci-l4-esa-merged-oi-v5.5-30dr	2182	-0.08	-0.15	0.48	0.51	0.39	0.289	0.28

► Table 2 is similar to Table 1 but considering only match-up pairs where $RR=0$ mm/h, $3 < U_{10} < 12$ m/s, $SST > 5^\circ\text{C}$, distance to coast > 800 km.

Table 2: Statistics of ΔSSS (Satellite - TSG (SAMOS)) - C1

Satellite products	#	Median	Mean	Std	RMS	IQR	r^2	Std*
smos-l2-v700	1245	-0.36	-0.38	0.67	0.77	0.89	0.274	0.67
smap-l2-rss-v6	596	0.10	0.08	0.28	0.29	0.36	0.496	0.27
smap-l2-rss-v6-40km	546	-0.04	-0.02	0.69	0.69	0.98	0.016	0.73
smap-l2-jpl-v5.0	603	0.14	0.16	0.45	0.48	0.62	0.099	0.46
aquarius-l2-or-v5	177	-0.14	-0.09	0.22	0.24	0.29	0.257	0.23
aquarius-l2-jpl-v5	185	0.00	0.05	0.28	0.28	0.35	0.228	0.27
smos-l3-catds-cpdc-v333-l2q	800	-0.12	-0.07	0.60	0.61	0.71	0.288	0.53
smos-l3-catds-cpdc-v332-9d	1933	-0.03	-0.03	0.29	0.29	0.43	0.485	0.32
smos-l3-catds-cpdc-v335-10d-25km	1933	-0.01	-0.06	0.35	0.35	0.49	0.339	0.38
smos-l3-catds-cpdc-v335-1m-25km	1933	-0.02	0.02	0.24	0.24	0.28	0.631	0.21
smos-l3-catds-locean-v9-9d	2709	-0.03	-0.06	0.32	0.32	0.43	0.415	0.32
smos-l3-catds-locean-v9-18d	2709	-0.07	-0.05	0.27	0.27	0.34	0.540	0.25
smos-l3-bec-v2-9d	1232	0.07	0.12	0.39	0.41	0.68	0.188	0.51
smap-l3-rss-v6-8dr	865	0.01	0.02	0.14	0.14	0.17	0.800	0.13
smap-l3-rss-v6-1m	865	0.02	0.04	0.26	0.27	0.28	0.675	0.21
smap-l3-jpl-v5.0-8dr	865	0.08	0.08	0.19	0.20	0.28	0.666	0.21
smap-l3-jpl-v5.0-1m	483	0.21	0.21	0.22	0.31	0.30	0.743	0.25
aquarius-l3-or-v5-7dr	483	-0.04	0.03	0.25	0.25	0.23	0.869	0.16
aquarius-l3-or-v5-1m	483	-0.05	0.04	0.27	0.28	0.28	0.804	0.18
aquarius-l3-or-v5-7dr-rain-mask	439	-0.04	0.02	0.25	0.25	0.23	0.874	0.16
aquarius-l3-or-v5-1m-rain-mask	483	-0.02	0.06	0.27	0.27	0.25	0.826	0.17
aquarius-l3-jpl-v5-7dr	483	0.11	0.13	0.25	0.28	0.33	0.760	0.24
aquarius-l3-jpl-v5-1m	483	0.10	0.19	0.24	0.30	0.30	0.816	0.20
smos-l4-bec-v2-1d	1739	0.15	0.13	0.35	0.38	0.65	0.319	0.45
smos-l4-cmems-catds-lops-oi-v346-1w	1618	0.01	0.00	0.24	0.24	0.36	0.667	0.27
smos-l4-cmems-cnr-v1-1d	1687	-0.09	-0.07	0.23	0.25	0.29	0.650	0.21
smos-l4-cmems-cnr-v1-1m	1687	-0.04	-0.03	0.22	0.22	0.29	0.694	0.22
cci-l4-esa-merged-oi-v4.41-7dr	1554	-0.07	-0.04	0.24	0.24	0.36	0.637	0.26
cci-l4-esa-merged-oi-v4.41-30dr	1558	-0.07	-0.04	0.25	0.25	0.36	0.601	0.27
smap-l4-esr-oi-v3-1d	4524	0.11	0.08	0.23	0.24	0.35	0.765	0.26
smap-l4-esr-oi-v3-1m	1131	0.04	0.09	0.23	0.24	0.35	0.750	0.25
aquarius-l4-iprc-v5-1w	551	-0.13	-0.06	0.24	0.25	0.20	0.813	0.12
aquarius-l4-iprc-v5-1m	551	-0.11	-0.04	0.22	0.22	0.18	0.887	0.13
cci-l4-esa-merged-oi-v5.5-7dr	1574	-0.06	-0.02	0.21	0.21	0.32	0.711	0.22
cci-l4-esa-merged-oi-v5.5-30dr	1566	-0.04	0.00	0.23	0.23	0.36	0.672	0.25

- Numerical values can be downloaded as csv files for [Table 1](#) and [Table 2](#).
- Figures using numerical values of Table 1 sorted by [MEDIANS](#), [MEANS](#), [IQR](#), [RMS](#), [STD](#), [R2](#) are also provided.
- Figures using numerical values of Table 2 sorted by [MEDIANS](#), [MEANS](#), [IQR](#), [RMS](#), [STD](#), [R2](#) are also provided.

Caution has to be made in the interpretation of the "ranking" between different satellite products in particular when looking at the dispersion parameters like the standard deviation (STD), or the interquartile range (IQR). Keep in mind that

low spatial and/or temporal resolution satellite SSS products tend to have lower dispersions than products at higher resolutions. For example, a level 2 (swath) product of a specific sensor will always have more dispersion than level 3 or 4 products where spatial and temporal averaging tend to reduce the instrumental noise and potential small scale variability. In general, products at $1^\circ \times 1^\circ$ spatial resolution have lower dispersion than products at $0.25^\circ \times 0.25^\circ$. Same result applies for monthly products compared to daily products.

5.2 Statistics derived for the different *in situ* databases

► Table 1 shows the mean, median, standard deviation (Std), root mean square (RMS), interquartile range (IQR), correlation coefficient (r^2) and robust standard deviation (Std*) of the match-up differences Δ SSS (Satellite - *in situ*) between **SMOS SSS L2 v700 (ESA)** and all the available *in situ* datasets derived over the SPURS 2 Pi-MEP region and for the full satellite product period and considering all match-up pairs satellite/*in situ* SSS values to derive the statistics:

Table 1: Statistics of Δ SSS (Satellite - *in situ*)

<i>in situ</i> database	#	Median	Mean	Std	RMS	IQR	r^2	Std*
argo	2655	-0.09	-0.10	0.63	0.64	0.79	0.384	0.59
tsg-gosud-research-vessel	645	-0.24	-0.15	0.64	0.66	0.93	0.003	0.65
tsg-gosud-sailing-ship	5143	0.12	0.26	0.70	0.75	0.80	0.232	0.52
tsg-samos	1582	-0.44	-0.49	0.71	0.86	0.94	0.206	0.72
drifter	45631	0.10	0.06	0.67	0.68	0.86	0.335	0.64
snake	1430319	0.13	0.12	0.62	0.63	0.90	0.161	0.67
saildrone-spurs2	2449	0.11	0.19	0.63	0.66	0.66	0.363	0.52
waveglider	258805	0.04	-0.05	0.63	0.63	0.81	0.510	0.57
seaglider	29211	0.09	0.03	0.66	0.66	0.83	0.497	0.60
saildrone	10202	0.19	0.11	0.78	0.79	1.07	0.164	0.81

► Table 2 is similar to Table 1 but considering only match-up pairs where $RR=0$ mm/h, $3 < U_{10} < 12$ m/s, $SST > 5^\circ\text{C}$, distance to coast > 800 km.

Table 2: Statistics of Δ SSS (Satellite - *in situ*)

<i>in situ</i> database	#	Median	Mean	Std	RMS	IQR	r^2	Std*
argo	1836	-0.06	-0.06	0.58	0.58	0.76	0.383	0.56
tsg-gosud-research-vessel	645	-0.24	-0.15	0.64	0.66	0.93	0.003	0.65
tsg-gosud-sailing-ship	4113	0.10	0.25	0.70	0.75	0.78	0.073	0.47
tsg-samos	1245	-0.36	-0.38	0.67	0.77	0.89	0.274	0.67
drifter	27541	0.11	0.11	0.58	0.59	0.75	0.389	0.56
snake	789026	0.11	0.12	0.60	0.61	0.93	0.138	0.70
saildrone-spurs2	1172	0.11	0.15	0.55	0.57	0.53	0.222	0.41
waveglider	172315	0.04	-0.01	0.56	0.56	0.75	0.552	0.54
seaglider	16526	0.11	0.08	0.57	0.58	0.73	0.574	0.54
saildrone	2800	0.54	0.52	0.54	0.75	0.65	0.512	0.48

► Numerical values can be downloaded as csv files for [Table 1](#) and [Table 2](#).

References

- Abderrahim Bentamy and Denis Croize Fillon. Gridded surface wind fields from Metop/ASCAT measurements. *Int. J. Remote Sens.*, 33(6):1729–1754, March 2012. ISSN 1366-5901. doi: [10.1080/01431161.2011.600348](https://doi.org/10.1080/01431161.2011.600348).
- Abderrahim Bentamy, Semyon A. Grodsky, James A. Carton, Denis Croizé-Fillon, and Bertrand Chapron. Matching ASCAT and QuikSCAT winds. *J. Geophys. Res.*, 117(C2), February 2012. ISSN 0148-0227. doi: [10.1029/2011JC007479](https://doi.org/10.1029/2011JC007479).
- Jacqueline Boutin, Jean-Luc Vergely, Emmanuel P. Dinnat, Philippe Waldteufel, Francesco D’Amico, Nicolas Reul, Alexandre Supply, and Clovis Thouvenin-Masson. Correcting sea surface temperature spurious effects in salinity retrieved from spaceborne l-band radiometer measurements. *IEEE Trans. Geosci. Remote Sens.*, pages 1–14, 2020. doi: [10.1109/tgrs.2020.3030488](https://doi.org/10.1109/tgrs.2020.3030488).
- Jaqueline Boutin, Y. Chao, W. E. Asher, T. Delcroix, R. Drucker, K. Drushka, N. Kolodziejczyk, T. Lee, N. Reul, G. Reverdin, J. Schanze, A. Soloviev, L. Yu, J. Anderson, L. Brucker, E. Dinnat, A. S. Garcia, W. L. Jones, C. Maes, T. Meissner, W. Tang, N. Vinogradova, and B. Ward. Satellite and In Situ Salinity: Understanding Near-Surface Stratification and Sub-footprint Variability. *Bull. Am. Meteorol. Soc.*, 97(8):1391–1407, 2016. ISSN 1520-0477. doi: [10.1175/bams-d-15-00032.1](https://doi.org/10.1175/bams-d-15-00032.1).
- Clément de Boyer Montégut, Gurvan Madec, A. S. Fischer, A. Lazar, and D. Ludicone. Mixed layer depth over the global ocean: An examination of profile data and a profile-based climatology. *J. Geophys. Res.*, 109(C12), December 2004. doi: [10.1029/2004jc002378](https://doi.org/10.1029/2004jc002378).
- Clément de Boyer Montégut, Juliette Mignot, Alban Lazar, and Sophie Cravatte. Control of salinity on the mixed layer depth in the world ocean: 1. General description. *J. Geophys. Res.*, 112(C6), June 2007. ISSN 0148-0227. doi: [10.1029/2006jc003953](https://doi.org/10.1029/2006jc003953).
- Ralph R. Ferraro. SSM/I derived global rainfall estimates for climatological applications. *J. Geophys. Res.*, 102(D14):16715–16736, 07 1997. doi: [10.1029/97JD01210](https://doi.org/10.1029/97JD01210).
- Ralph R. Ferraro, Fuzhong Weng, Norman C. Grody, and Limin Zhao. Precipitation characteristics over land from the NOAA-15 AMSU sensor. *Geophys. Res. Lett.*, 27(17):2669–2672, 2000. doi: [10.1029/2000GL011665](https://doi.org/10.1029/2000GL011665).
- Fabienne Gaillard, Thierry Reynaud, Virginie Thierry, Nicolas Kolodziejczyk, and Karina von Schuckmann. In Situ-Based Reanalysis of the Global Ocean Temperature and Salinity with ISAS: Variability of the Heat Content and Steric Height. *J. Clim.*, 29(4):1305–1323, February 2016. ISSN 1520-0442. doi: [10.1175/jcli-d-15-0028.1](https://doi.org/10.1175/jcli-d-15-0028.1).
- Robert J. Joyce, John E. Janowiak, Phillip A. Arkin, and Pingping Xie. CMORPH: A Method that Produces Global Precipitation Estimates from Passive Microwave and Infrared Data at High Spatial and Temporal Resolution. *J. Hydrometeorol.*, 5(3):487–503, June 2004. doi: [10.1175/1525-7541\(2004\)005\(0487:camtpg\)2.0.co;2](https://doi.org/10.1175/1525-7541(2004)005(0487:camtpg)2.0.co;2).
- Nicolas Kolodziejczyk, Gilles Reverdin, and Alban Lazar. Interannual Variability of the Mixed Layer Winter Convection and Spice Injection in the Eastern Subtropical North Atlantic. *J. Phys. Oceanogr.*, 45(2):504–525, Feb 2015. ISSN 1520-0485. doi: [10.1175/jpo-d-14-0042.1](https://doi.org/10.1175/jpo-d-14-0042.1).

Christian Kummerow, Y. Hong, W. S. Olson, S. Yang, R. F. Adler, J. McCollum, R. Ferraro, G. Petty, D-B. Shin, and T. T. Wilheit. The Evolution of the Goddard Profiling Algorithm (GPROF) for Rainfall Estimation from Passive Microwave Sensors. *J. Appl. Meteorol.*, 40(11): 1801–1820, 2001. doi: [10.1175/1520-0450\(2001\)040<1801:TEOTGP>2.0.CO;2](https://doi.org/10.1175/1520-0450(2001)040<1801:TEOTGP>2.0.CO;2).

Shawn R. Smith, Jeremy J. Rolph, Kristen Briggs, and Mark A. Bourassa. Quality-Controlled Underway Oceanographic and Meteorological Data from the Center for Ocean-Atmospheric Predictions Center (COAPS) - Shipboard Automated Meteorological and Oceanographic System (SAMOS), 2009. doi: [10.7289/v5qj7f8r](https://doi.org/10.7289/v5qj7f8r).